



# Antimony-based intermetallic compounds for lithium-ion and sodium-ion batteries: synthesis, construction and application

Wen Luo, Jean-Jacques Gaumet, Li-Qiang Mai\*

Received: 16 December 2016/Revised: 21 January 2017/Accepted: 13 March 2017/Published online: 4 May 2017  
© The Nonferrous Metals Society of China and Springer-Verlag Berlin Heidelberg 2017

**Abstract** The development of alternative electrode materials with high energy densities and power densities for batteries has been actively pursued to satisfy the power demands for electronic devices and hybrid electric vehicles. Recently, antimony (Sb)-based intermetallic compounds have attracted considerable research interests as new candidate anode materials for high-performance lithium-ion batteries (LIBs) and sodium-ion batteries (SIBs) due to their high theoretical capacity and suitable operating voltage. However, these intermetallic systems undergo large volume change during charge and discharge processes, which prohibits them from practical application. The rational construction of advanced anode with unique structures has been proved to be an effective approach to enhance its electrochemical performance. This review highlights the recent progress in improving and understanding the electrochemical performances of various Sb-based intermetallic compound anodes. The developments of synthesis and construction of Sb-based intermetallic compounds are systematically summarized. The electrochemical performances of various Sb-based

intermetallic compound anodes are compared in its typical applications (LIBs or SIBs).

**Keywords** Antimony; Intermetallic compound; Alloy; Anode; Sodium-ion battery; Lithium-ion battery

## 1 Introduction

Energy conversion and storage have become key issues with concerns to our welfare in modern society. For several decades, lithium-ion batteries (LIBs) have gained much importance for portable electronic devices, hybrid electric vehicles and backup electricity storage units for renewable energy sources [1–3]. Recently, owing to the great concerns to the limited lithium (Li) resources on earth, sodium-ion batteries (SIBs) have captured intensive research interests as one of the viable alternatives to LIBs because of its abundant sodium (Na) reserves and low-voltage operation [4–6]. Moreover, researches show that for cathode materials, sodium intercalation chemistry shares similar redox principle to LIB systems upon electrochemical process, which makes it possible to employ the same compounds in both LIB and SIB systems [7, 8].

However, how to prepare high-performance anode materials with high energy density, suitable lithiation or sodiation potential and long cycle life is still a challenge. For instance, graphite, which is used as the anode material for commercial rechargeable LIBs, cannot fulfill the requirement for higher output capacity due to its insufficient theoretical capacity of  $372 \text{ mAh}\cdot\text{g}^{-1}$  [9, 10]. Recently, antimony (Sb)-based nanocomposites have demonstrated impressive performances by sustaining reversible capacities between 500 and  $800 \text{ mAh}\cdot\text{g}^{-1}$  over

---

W. Luo, L.-Q. Mai\*  
State Key Laboratory of Advanced Technology for Materials  
Synthesis and Processing, Wuhan University of Technology,  
Wuhan 430070, China  
e-mail: mlq518@whut.edu.cn

W. Luo, J.-J. Gaumet  
Laboratory of Chemistry and Physics: Multiscale Approach to  
Complex Environments (LCP-A2MC), University of Lorraine,  
Metz 57070, France

L.-Q. Mai  
Department of Chemistry, University of California, Berkeley,  
California 94720, USA

numerous cycles during the lithiation or sodiation processes [11–16]. With respect to Sb-based intermetallic compounds, these alloys are featured with merits as promising anodes for LIBs and SIBs. Taking SnSb intermetallic alloys as LIBs anode for example [17, 18], (1) both Sn ( $\text{Li}_{4.4}\text{Sn}$ ,  $990 \text{ mAh}\cdot\text{g}^{-1}$ ) and Sb ( $\text{Li}_3\text{Sb}$ ,  $660 \text{ mAh}\cdot\text{g}^{-1}$ ) elements can alloy/de-alloy reversibly, contributing to a high lithium storage capacity; (2) the volume variations of the cycled alloys due to the alloying/de-alloying of  $\text{Li}^+$  can be partially accommodated by a highly dispersed ductile Sn phase; (3) high energy density can be achieved in a SnSb anode-based full cell because of its suitable redox potential. Despite these desirable features, the practical capacity and cycling performance of these Sb-based alloys are often limited by the cracking and pulverization of active anode particles during long-term cycling processes [19]. A representative illustration of the reaction mechanism of Sb-based anode is shown in Fig. 1. Those Sb-based intermetallic anodes which undergo an alloying or conversion reaction would suffer major structural changes during charge and discharge process.

Recently, the development of nanoscience and nanotechnology has provided the possibility to tailor the physical or chemical properties and improve the performance of functional materials. Most of Sb intermetallic compounds are found to present excellent electrochemical performance through novel structure design and composition optimization. As summarized in some recent review articles, nanostructured electrode materials are able to manifest superior electrochemical properties compared to their bulk counterparts [20–22]. And to date, several review articles summarizing the application of alloy anode for LIBs or SIBs have already been reported by Park and coworkers [23], Obrovac and Chevrier [24] and Zhang [25]. But there are few reviews that systematically summarize the synthesis and construction of Sb-based intermetallic compounds for LIBs and SIBs. Herein, we mainly

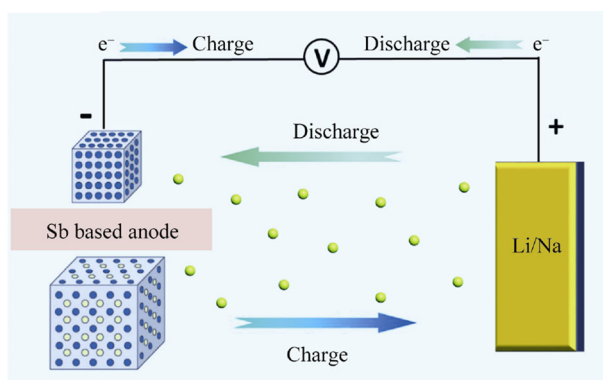


**Fig. 1** Illustration of charge–discharge process involved in rechargeable batteries consisting of Sb-based intermetallic compound anode and lithium or sodium metal cathode

review the recent progress in improving and understanding the electrochemical performance of various Sb-based intermetallic compound anodes. The developments of synthesis and construction of Sb-based intermetallic compounds are systematically summarized. The electrochemical performances of various Sb-based intermetallic compound anodes are compared in its typical electrochemical energy storage applications (LIBs or SIBs).

## 2 Construction and synthesis of Sb-based alloy for energy storage

In this article, we will review some typical novel synthesis methods of Sb-based intermetallic compound in recent years. Most commonly utilized strategies to fabricate high-performance nanostructured electrode materials are solvothermal/hydrothermal synthesis. Because of its facility, inexpensive equipment involved and moderate reaction condition, these kinds of synthesis methods gain much interest. Zhao et al. have described the preparation of the nanocrystalline  $\text{CoSb}_2$  by a solvothermal method at various temperatures [26, 27]. It was found that  $\text{CoSb}_2$  is highly crystallized at  $190^\circ\text{C}$  and with almost a single-phase structure [27]. The produced  $\text{CoSb}_2$  nanocrystals are composed of small granules in the size of 20–30 nm and some large aggregates. By modifying synthesis condition, they further synthesized  $\text{CoSb}_3$  nanocrystals with the aggregates in size of above 60 nm [28]. They also found that these  $\text{CoSb}_3$  can be bounded well with multiwall carbon nanotubes (MWCNTs) by grinding with an agate mortar [29]. Similarly,  $\text{NiSb}$  and  $\text{NiSb}_2$  particles in large aggregates are also synthesized by Zhao et al. via the solvothermal route [30, 31]. Interestingly,  $\text{NiSb}$  [30] and  $\text{NiSb}_2$  [31] products can be easily controlled by using different reducing agents at a lower temperature to realize its better disperse with the particle size in 60–80 nm. For the solvothermal/hydrothermal synthesis of Sb-based intermetallic compounds, other advanced strategies can be easily achieved such as template-assisted method. Huang et al. reported hollow  $\text{Cu}_2\text{Sb}@C$  core–shell nanoparticles obtained by controlling the amount of  $\text{CuCl}_2$  and time of replacement reaction via a simple polyol approach [32]. In this work, Sb particles not only act as antimony sources but also play a role as a sacrifice template (Fig. 2a). As time passes, Sb particles are gradually consumed, and Ostwald ripening occurs as  $\text{Cu}_2\text{Sb}$  around the surface of the Sb forms a shell, finally leaving  $\text{Cu}_2\text{Sb}@C$  hollow core–shell nanoparticles with an average diameter of 25 nm (Fig. 2b, c).

Solution chemical reduction route is often used to synthesize nanosized materials with uniform size distribution at moderate temperature and lower pressure compared to a

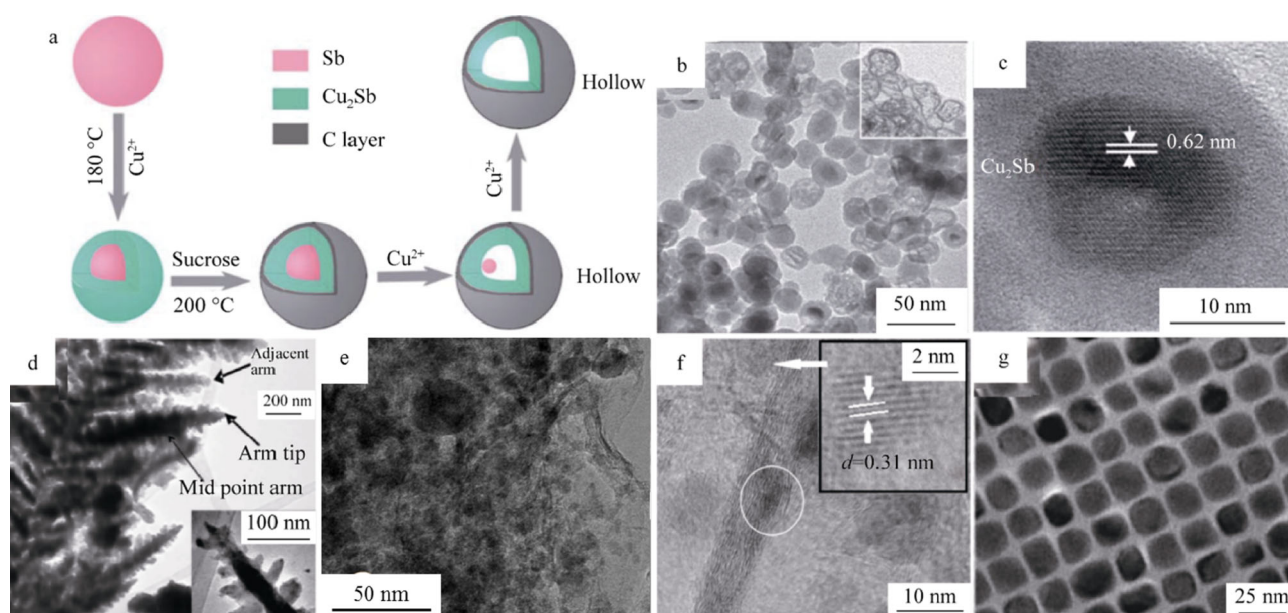


**Fig. 2** Schematic diagram for formation of  $\text{Cu}_2\text{Sb}@C$  nanoparticles evolved from Sb nanoparticles **a**, transmission electron microscopy (TEM) images of hollow  $\text{Cu}_2\text{Sb}@C$  core-shell nanoparticles **b**, **c**, as-precipitated (un-annealed) InSb morphology and annealed microstructure (inset) **d**, TEM image of SnSb/graphene composite **e**, high-resolution TEM image showing SnSb nanoparticles and graphene sheets **f** and TEM image of  $\sim 20$ -nm SnSb NCs **g**

typical solvothermal/hydrothermal synthesis. Sarakonsri and Johnson [33] reported an intriguing synthesis of dendrite-like InSb (Fig. 2d),  $\text{Cu}_6\text{Sn}_5$  and  $\text{Cu}_2\text{Sb}$  anodes via a solution chemical reduction route synthesis. It is found heterogeneous redox reactions at the surface of the Zn particles resulted in fern-like dendritic structures with high specific surface areas. In the presence of sodium citrate as a complexing agent and different reducing agents, nanoscale size  $\text{Cu}_2\text{Sb}$  particles can be achieved [34]. To achieve SnSb-based alloy, co-precipitation method is often involved in most of the articles [18, 35–40]. The variety of synthesis parameters have great effects on the morphology of the obtained anode materials; for instance, small SnSb particle size with low crystallinity (reduced by  $\text{NaBH}_4$ ), dendrite-like SnSb bulks (reduced by Zn in aqueous solution) and irregular bulk SnSb particles (reduced by Zn in glycol) were synthesized, respectively [39]. Carbon nanotube or graphene modification can be facilely composited in SbSn-based anode through a moderate solution chemical reduction route, such as spherical nano-SnSb/mesoporous carbon microbeads (MCMB)/carbon core-shell composite [41], SnSb/CNT composite [40, 42, 44, 45],  $\text{Sn}_x\text{Sb}$ -graphene-carbon nanofibers [43],  $\text{SnSb}_{0.5}$ /CNT composite [38] and SnSb/hard carbon sphere composite [46]. The SnSb/graphene composite with three-dimensional (3D) porous structure was prepared via an in situ chemical reduction method (Fig. 2e, f) [47, 48]. The as-synthesized SnSb/graphene composite has an excellent electrical conductivity; the corrugated and stacked graphene sheets also

provide a porous buffer matrix on the macrodomain, thus significantly enhancing the capacity retention, cycling performance and rate capability. Recently, Kovalenko et al. demonstrated an inexpensive and scalable synthesis of SnSb nanocrystals with 10–30 nm in size [49] and an intriguing monodisperse  $\sim 20$ -nm-sized SnSb colloidal (Fig. 2g) [50] under certain designed reducing condition. The important advantages of this method over previous solution syntheses are its nearly quantitative reaction yield and its avoidance of the use of surfactants.

High-energy mechanical milling (HEMM) technique is attractive for the construction of high-performance anode materials, since this method yields well-distributed, nano-sized metal or alloy crystallites in the certain matrix via the repeated flattening, welding, fracturing and rewelding of the particles [51]. A  $\text{Zn}_3\text{Sb}_4$ /graphite composite [52] was synthesized via HEMM for LIBs. The electrode behavior has been largely improved when graphite additives were employed. Park and Sohn conducted a novel research on quasi-intercalation and facile amorphization in layered ZnSb for LIBs [53]. By the HEMM technique, 3-nm-sized ZnSb nanocrystallites were uniformly distributed within a carbon matrix, and the achieved product exhibits excellent electrochemical properties (Fig. 3a–c). Another example deserves mentioning is the construction of the porous structured SnSb/C materials after HEMM treatment [54]. In this work,  $\text{MgCl}_2$  in the milled SnSb/ $\text{MgCl}_2$ /C composite was washed by solution mixed with ethanol (EtOH) and distilled water (Fig. 3d). And finally a unique structure

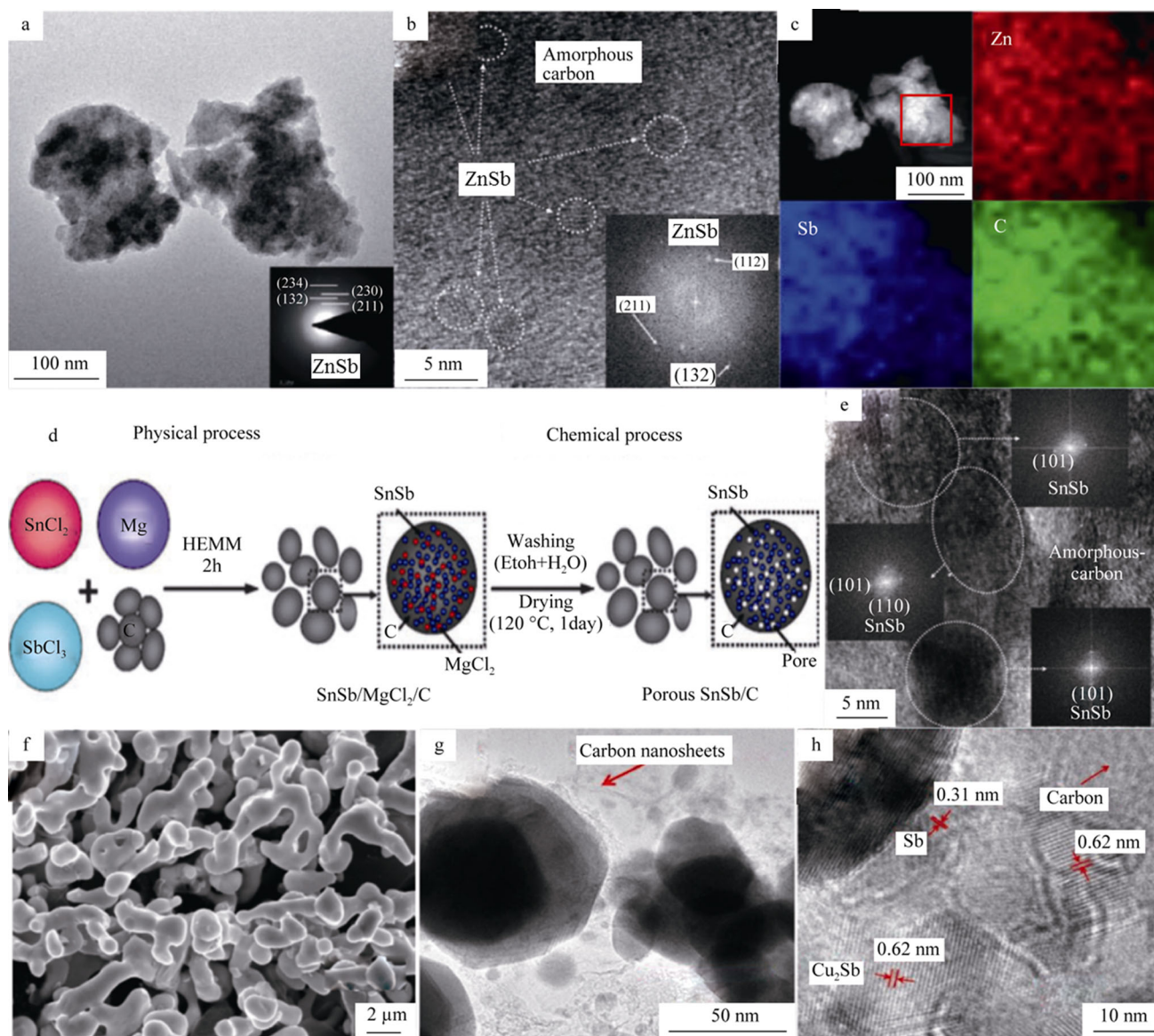


**Fig. 3** TEM image and corresponding lattice spacing **a**, high-resolution transmission electron microscopy (HRTEM) image **b** and energy-dispersive spectroscopy (EDS) mappings **c** of amorphized ZnSb/C nanocomposite, schematic diagram for synthesis of porous structured SnSb/C nanocomposites **d**, HRTEM images and corresponding lattice spacing of porous structured SnSb/C nanocomposites **e**, scanning electron microscopy (SEM) image of worm-like CoSb powders **f** and TEM images of Sb/Cu<sub>2</sub>Sb/C composite **g**, **h**

of ~11-nm-sized SnSb nanocrystallines embedded in porous carbon matrix composite was achieved (Fig. 3e). Various nanostructured SnSb or SnSb/C composites were synthesized via HEMM technique [55–58]. In the SnSb/C composite, 2–3 nm-sized SnSb nanocrystallites are uniformly distributed within a carbon matrix which can result in an exceptionally high capacity (544 mAh·g<sup>-1</sup>, almost double that of intercalation carbon materials), good rate capacity and cyclability for SIBs [58]. TiC is also utilized as a buffer material in some SnSb–TiC–C composites via HEMM technique [56, 59, 60]. Manthiram et al. demonstrated that the buffer matrix of TiC and carbon in the

nanocomposite alloy anodes accommodates the large volume change occurring during the charge and discharge process and leads to enhanced cyclability compared to pure SnSb anode [59].

Thermal sintering or heat treatment method has been intensively employed to synthesize alloy materials. It should be noted that in most of the cases, thermal sintering is often used combined with preceding hydrothermal synthesis or HEMM treatment to increase crystallization, to in situ reduce and carbonize composite or to reinforce structure. Microsized CoSb alloy powders were synthesized by carbothermal reduction method from oxides of Co

and Sb [61]. Sb is firstly reduced from  $\text{Sb}_2\text{O}_3$ , followed by the reduction of Co from  $\text{Co}_3\text{O}_4$  and the alloying of Sb with Co. The liquid feature of Sb at synthesis temperature renders the CoSb particles with a worm-like shape (Fig. 3f). For the preparation of desired alloy, sample can be facily synthesized according to its stoichiometric ratio of each element by heat treatment such as the synthesis of  $\text{TiSb}_2$  nanoparticles [62] and  $\text{SnSb}$  microsized particles [63]. Multicomponent alloys can also be easily synthesized through thermal sintering. Microscaled Sn–Sb–Ni alloy composites were synthesized via carbothermal reduction from corresponding oxides of Sn, Sb and Ni directly [64]. The ductile Ni can buffer the big volume change of electrode and thus make great contribution to the cycling stability of electrode. Ma et al. fabricated  $\text{Sb}/\text{Cu}_2\text{Sb}/\text{C}$  composite using a high-temperature solid-phase method [65]. This method involves the synchronously formed amorphous carbon layers matrix and  $\text{Cu}_2\text{Sb}$  particles (Fig. 3g, h) that can effectively accommodate the volume changes of Sb during electrochemical cycles and improve the conductivity of the  $\text{Sb}/\text{Cu}_2\text{Sb}/\text{C}$  electrode.

Electrodeposition technique plays a vital role in the fabrication of various nanostructures with high aspect ratio structures whose dimensions can be easily controlled and fine-tuned. CoSb nanowire arrays with different degrees of order were synthesized by Yang et al. [66] through electrodeposition. Yang et al. [67] also synthesized  $\text{Ni}_2\text{Sb}_5$  nanowires with a diameter of 80 nm, and these uniform

nanowires parallel to each other and thoroughly flush at the bottom (Fig. 4a, b). ZnSb nanotubes were grown through a template-free electrodeposition method under over-potential conditions (Fig. 4c, d) [68]. The growth of the nanotubes was attributed to the template effect from  $\text{H}_2$  bubbles. Owing to their hollow structures, the ZnSb nanotubes depicted better Li-ion storage performance compared to that of ZnSb nanoparticles deposited under different conditions. Electrodeposition technique has also been regarded as an efficient tool to fabricate thin-film anode for LIBs or SIBs.  $\text{Cu}_9\text{Sb}_2$  thin films have been manufactured via electrodeposition with nanoflake or nanoparticle morphology on the surface of film (Fig. 4e, f) [69]. Prieto et al. reported one kind of  $\text{Cu}_2\text{Sb}$  thin film possessed a uniform surface with a thickness of  $32.4 \mu\text{m}$  [70]. Notably, the electrodeposition of  $\text{Cu}_2\text{Sb}$  directly onto conducting substrates represents excellent electrical contact to a substrate, which is critical for further battery testing.

Galvanic replacement has attracted much interest as a low-temperature and facile synthesis of nanoarchitected alloy materials [71–73]. Ji et al. introduced galvanic replacement to synthesize dispersive hollow NiSb spheres for LIBs [74]. These NiSb nanospheres were featured with a diameter of 70–100 nm and wall thickness of 15 nm. The composition and morphology of the ZnSb nanostructures could be tuned by varying the molar ratio of the precursors (e.g.,  $\text{ZnCl}_2$ :  $\text{SbCl}_3$ ), the deposition potentials and the

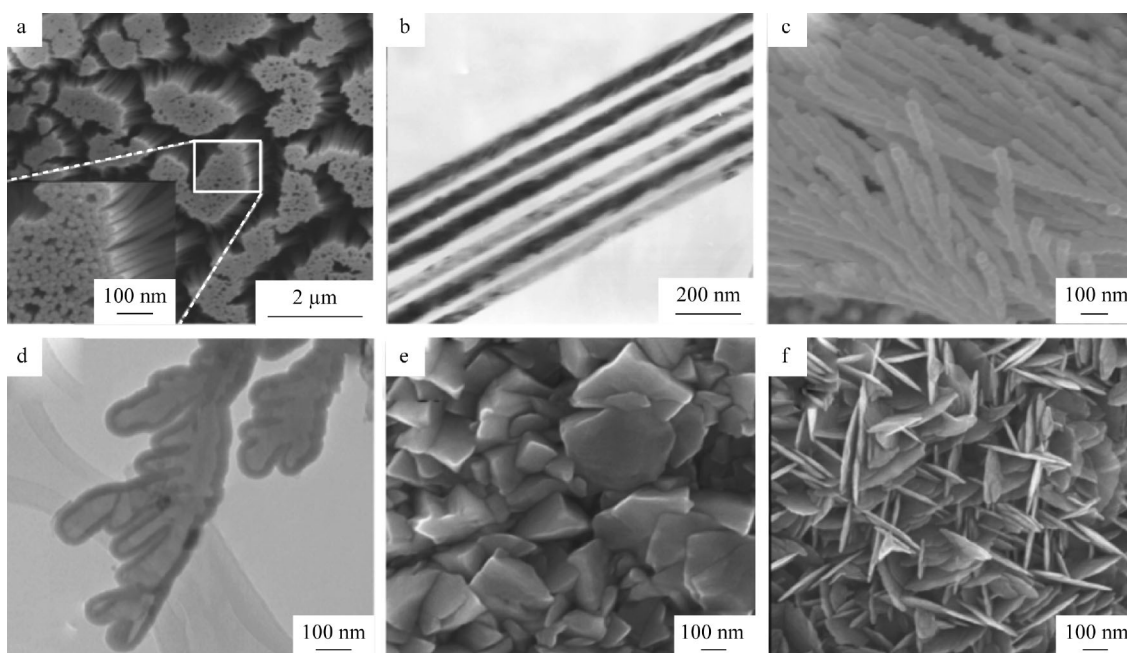


**Fig. 4** Typical morphologies of materials synthesized by electrodeposition method: **a** bottom-view SEM image (inset being a magnified local SEM image) and **b** TEM image of as-prepared  $\text{Ni}_5\text{Sb}_2$  nanowires array, **c** SEM image and **d** TEM image of electrodeposited ZnSb nanotubes and SEM images of deposited  $\text{Cu}_2\text{Sb}$  film **e** before heat treatment and **f** after heat treatment

substrate roughness. It can be concluded that the formation of wires is due to the substrate effect. 3D interconnected NiSb intermetallic hollow nanospheres [15] for SIBs were prepared involving crystallized 3D interconnected Ni nanospheres precursor and subsequent galvanic replacement reaction involving Sb ions (Fig. 5a–f). The hollow structure of nanospheres and 3D interconnected channels was verified to not only buffer the huge volume change and reduce the diffusion induced stress, but also facilitate the diffusion of  $\text{Na}^+$ .

Chemical vapor deposition (CVD) has been widely used as a versatile method for preparing advanced nanomaterials with complex architectures.  $\text{Cu}_{11}\text{Sb}_3$  nanowires (NWs),  $\text{Cu}_2\text{Sb}$  nanoparticles (NPs) or pure Sb nanoplates were obtained via CVD technique [75]. Zheng et al. demonstrated the CVD growth of several novel one-dimensional (1D)  $\text{Zn}_4\text{Sb}_3$  structures, including nanotubes (Fig. 5g), nanowires (Fig. 5h) and nanorods (Fig. 5i), directly on a

Cu foil [76]. It has been verified in this work that the 1D transport nature and the tubular structures of the obtained  $\text{Zn}_4\text{Sb}_3$  nanotubes offer excellent anode capacity and cycling stability compared to  $\text{Zn}_4\text{Sb}_3$  nanowires and  $\text{Zn}_4\text{Sb}_3$  nanorods. Guo et al. prepared SnSb-core/carbon-shell nanocables directly anchored on graphene sheets (GS) by the hydrothermal technique and CVD [77]. The good sodium storage performance of the as-synthesized SnSb/CNT@graphene can be attributed to the efficient buffering provided by the outer carbon nanocable layer and the graphene protection from the agglomeration of SnSb particles, as well as its high conductivity.

Electrospinning has been widely used as a convenient and versatile method for preparing 1D nanomaterials with controllable lengths, diameters and composition [78, 79]. Bhattacharyya et al. introduced 1D assembly of crystalline single-phase SnSb alloy nanoparticles inside porous carbon fibers synthesized by using the electrospinning technique

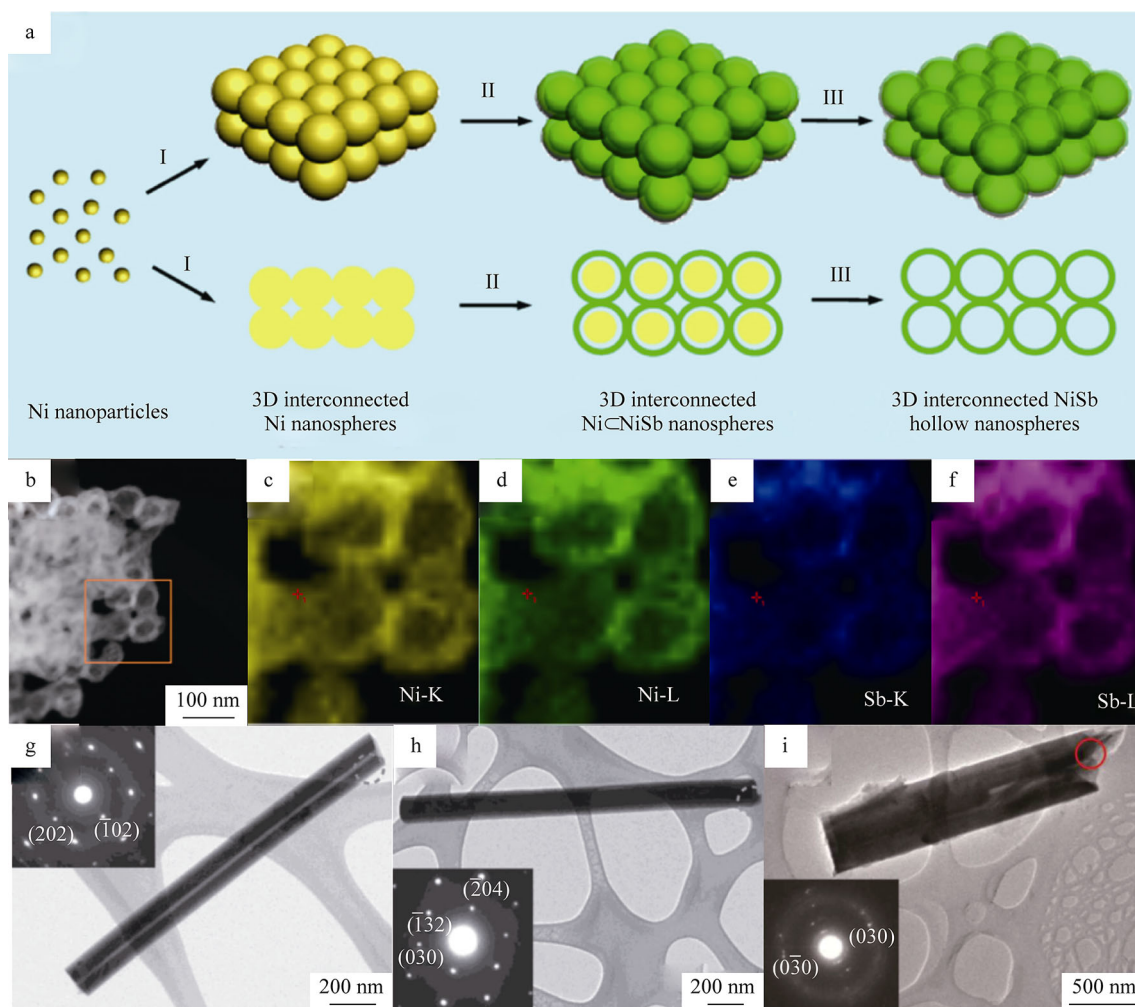


**Fig. 5** Schematic illustration of fabrication of 3D interconnected NiSb hollow nanospheres **a**, dark field TEM image **b** and corresponding elemental mapping of 3D interconnected NiSb hollow nanosphere for Ni–K **c**, Ni–L **d**, Sb–K **e**, Sb–L **f** edges; TEM images of  $\text{Zn}_4\text{Sb}_3$  g nanotube, **h** nanowire and **i** nanorod deposited on a copper foil by CVD

(employing nonoxide precursors) followed by an in situ carbonization and reduction strategy [80]. The presence of carbon in SnSb–C completely nullifies the conventional requirement of other carbon forms during cell electrode assembly. Liu et al. also reported a carbon nanofiber (CNF)-supported SnSb nanocomposite as anodes for enhanced sodium storage performance using electrospinning and a subsequent thermal treatment processes [81]. The highly dispersed SnSb nanoparticles with an average size of about 30 nm can be encapsulated in porous carbon nanofibers. 1D SnSb–C nanofibers can be transformed to 3D interconnected carbon network encapsulating SnSb particles by adjusting carbonization time and temperature [82].

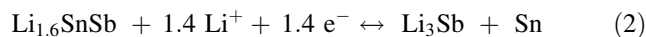
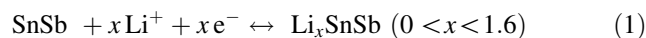
Besides, several conventional methods for metal manufacture are usually applied to synthesize Sb-based intermetallic compounds, such as hot-pressed method, vacuum melting, melt spinning method and magnetron sputtering.  $Zn_4Sb_3$  composite was prepared through hot-pressed method for the investigation of LIBs anode [83]. Zn and Sb shots in stoichiometric ratio were melted in sealed quartz ampoules. The melts should be held at 1023 K for about 2 h for homogenization and quenched in water.  $\beta$ - $Zn_4Sb_3$  [84],  $Zn_4Sb_3/C$  or  $CoSb_3/C$  composites [85] were obtained via vacuum melting process. Although the reported average particle sizes of the  $Zn_4Sb_3/C$  alloys are about 100 nm, most of them prepared by melting process tend to aggregate into large granule, which might have an inferior influence on its electrochemical performance. In one typical melt spinning of SnSb/CNTs composite [42], the SnSb particles were finely encrust within the mesh-like CNT framework. And this melt-spun SnSb/CNTs composite exhibits impressive rate performance, e.g., high reversible capacity of  $522 \text{ mAh}\cdot\text{g}^{-1}$  is obtainable at a high current density of  $\sim 3300 \text{ mA}\cdot\text{g}^{-1}$  (4C). Magnetron sputtering has been considered a necessary technique to manufacture alloy materials. Baggetto and coworkers reported the properties of magnetron-sputtered AlSb thin films [86] and  $Mo_3Sb_7$  thin films [87] during the electrochemical reactions with Li and Na.  $Mo_3Sb_7$  thin films are composed of small agglomerated domains with a surface morphology that follows the roughened Cu substrate. Impressively, the as-deposited  $Mo_3Sb_7$  films retain large capacities of about 310 and  $280 \text{ mAh}\cdot\text{g}^{-1}$  at very high rates of 100 and 30 C rate currents for Li and Na, respectively.

### 3 Electrochemical performance of Sb-based alloy

#### 3.1 Sn–Sb alloys

Sn–Sb-based alloys have drawn great research interest emphasized by an increasing number of publications. The choice of the SnSb system stems from several synergistic

effects between Sn and Sb [88–90]. First, both components of this alloy contribute to its high theoretical capacity of  $824 \text{ mAh}\cdot\text{g}^{-1}$  illustrated as follows:



Similarly, the theoretical maximum capacity for Na-ion storage in SnSb is  $752 \text{ mAh}\cdot\text{g}^{-1}$  based on the formation of  $\text{Na}_3\text{Sb}$  and  $\text{Na}_{3.75}\text{Sn}$  [57, 91]. Reducing particle size of SnSb alloy anodes could enhance morphological stability and thus improve the cycling performance. Lithium-ion storage in  $\sim 20$ -nm-sized SnSb colloidal [49] is characterized by capacities close to the theoretical maximum, with an average value of  $760 \text{ mAh}\cdot\text{g}^{-1}$  for 100 cycles at a high current density of  $1000 \text{ mA}\cdot\text{g}^{-1}$  (Fig. 6a). For sodium-ion storage, lower capacities are obtained, but with higher relative capacity retention upon cycling (Fig. 6b). More importantly, a full-cell measurement was conducted with these  $\sim 20$ -nm-sized SnSb nanocrystals (NCs). The first results from Li-ion and Na-ion full-cell experiments, using  $\text{LiCoO}_2$  and  $\text{Na}_{1.5}\text{VPO}_{4.8}\text{F}_{0.7}$  as the cathodes, indicate the stable cycling performance of SnSb NCs with specific Li- and Na-ion anodic capacities of  $600 \text{ mAh}\cdot\text{g}^{-1}$  (Fig. 6c) and  $400 \text{ mAh}\cdot\text{g}^{-1}$  (Fig. 6d), respectively. The Li-ion storage properties of monodisperse SnSb-alloyed NCs are enhanced due to the combination of high cycling stability of Sb with higher specific Li-ion storage capacity of Sn [50]. In particular, stable capacities of above  $580 \text{ mAh}\cdot\text{g}^{-1}$  were obtained at 20C rates for LIBs (Fig. 6e). Furthermore, Na-ion storage capacities of  $>350$  and  $>200 \text{ mAh}\cdot\text{g}^{-1}$  were obtained at 1C and 20C rates, respectively (Fig. 6f).

The combination of the alloy and the carbon in a designed structure shows great potential for improving the cycle life and rate capability. Kalisvaart et al. provided the first report on several compositions of ternary Sn–Ge–Sb thin-film alloys for application as SIBs anode [11]. This alloy has an initial reversible specific capacity of  $833 \text{ mAh}\cdot\text{g}^{-1}$  (at  $85 \text{ mA}\cdot\text{g}^{-1}$ ) and  $662 \text{ mAh}\cdot\text{g}^{-1}$  after 50 charge and discharge cycles. Specifically,  $\text{Sn}_{50}\text{Ge}_{25}\text{Sb}_{25}$  also shows excellent rate capability, displaying a stable capacity of  $381 \text{ mAh}\cdot\text{g}^{-1}$  at a current density of  $8500 \text{ mA}\cdot\text{g}^{-1}$  ( $\sim 10\text{C}$ ). A survey of published literature indicates that  $833 \text{ mAh}\cdot\text{g}^{-1}$  is among the highest reversible capacities reported for a Sn-based SIBs anode, while  $381 \text{ mAh}\cdot\text{g}^{-1}$  represents the optimum fast charge value. The lithiation capacity of Sn–Ni–Sb multicomponent alloy [64] was  $530 \text{ mAh}\cdot\text{g}^{-1}$  in the first cycle and maintained at  $370$ – $380 \text{ mAh}\cdot\text{g}^{-1}$  in the following cycles. The ductile Ni can buffer the big volume change of electrode and thus make great contribution to the cycling stability of

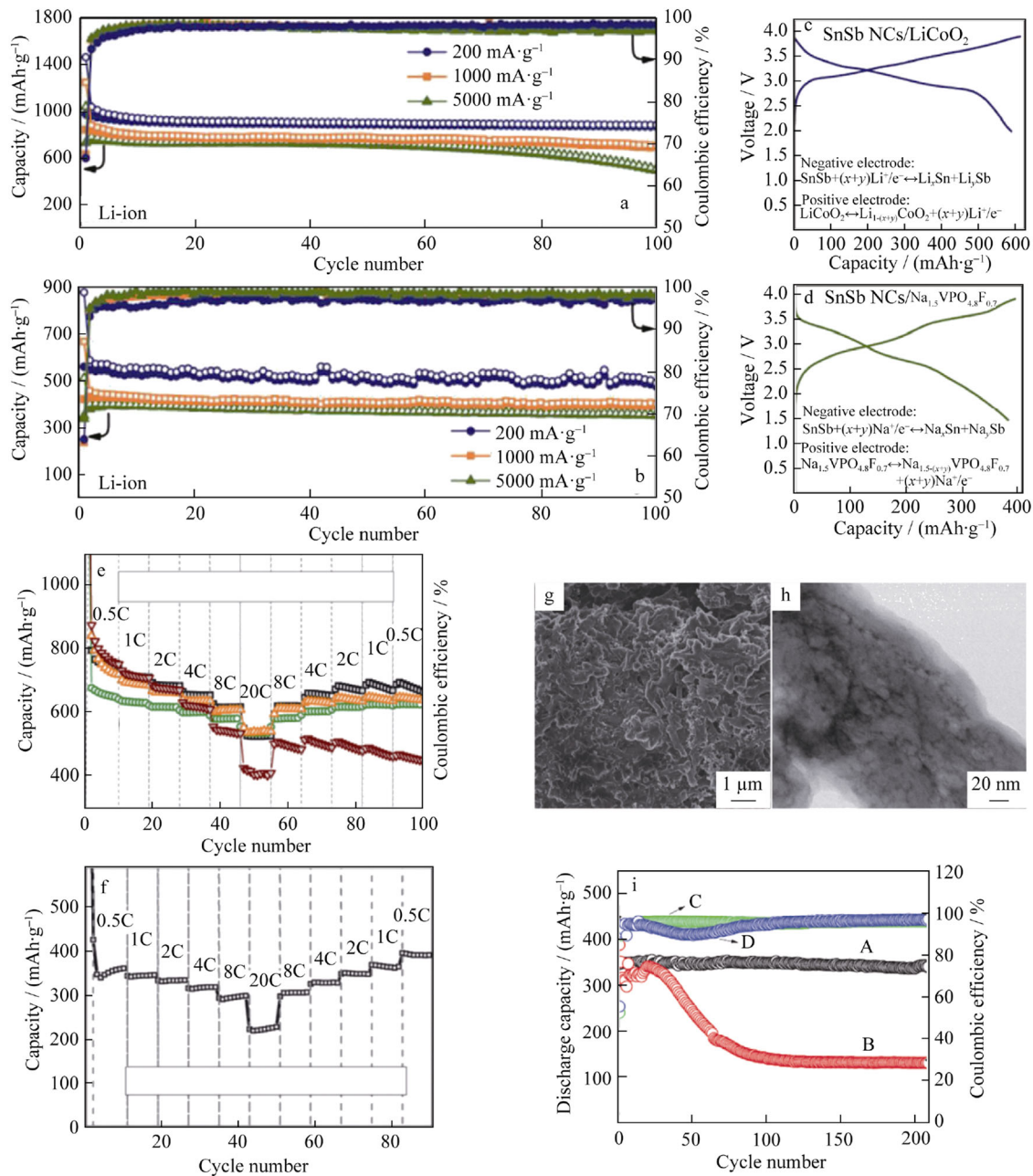


**Fig. 6** Capacity retention for SnSb NCs in **a** Li-ion and **b** Na-ion half cells, electrochemical performance of SnSb NCs in **c** lithium-ion full cells and **d** sodium-ion full cells using  $\text{LiCoO}_2$  and  $\text{Na}_{1.5}\text{VPO}_{4.8}\text{F}_{0.7}$  as cathode material; rate capability tests (0.5–20, 1C =  $660 \text{ mA}\cdot\text{g}^{-1}$ ) **e** for Li-ion anodes composed of SnSb, Sn and Sb NCs and **f** for Na-ion anodes comprising SnSb NCs; **g** SEM image and **h** TEM image of porous CNF-SnSb nanocomposite electrodes after 80 charge–discharge cycles at 0.2C in FEC-containing electrolyte; **i** cycling performance (Curves A, B) and corresponding Coulombic efficiency (Curves C, D) of porous CNF-SnSb electrodes in FEC-containing (Curves A, C) and FEC-free electrolyte (Curves B, D)

electrode. SnSb–TiC–C nanocomposite offers high volumetric capacity of  $1300 \text{ mAh}\cdot\text{m}^{-3}$  due to high tap density [56]. The buffer matrix of TiC and carbon in the nanocomposite alloy anodes accommodates the large volume change occurring during the charge and discharge process and leads to enhanced cyclability compared to pure SnSb anodes as well as previously published SnSb

composites. The improvement was attributed to the well-dispersed nanocrystalline Sb and the inactive TiC within the amorphous carbon matrix.

Carbon or graphene modification has been proven as an efficient strategy to improve conductivity and rate capability. It was found that depositing nanosized alloy particles on the surface of a stable frame NCs such as MCMBs

[36, 41], with larger particle size uniformly and separately, is an effective method to achieve higher Li storage capacity, better cyclic performance and higher discharge and charge efficiency simultaneously. Some graphene-modified SnSb anodes [92–94] also exhibited good electrochemical performance.

Moreover, an investigation by Liu et al. addressed the importance of electrolyte additive for better SnSb energy storage performance [81]. It has been proven that the presence of fluoroethylene carbonate (FEC) in electrolytes can prevent electrolyte decomposition and lead to the formation of thin, uniform, flexible and thus beneficial solid electrolyte interphase (SEI) films and uniform surface chemistry on the cycled electrode surfaces (Fig. 6g, h), which can modify the surface passivation. They further test the electrospun SbSn-C nanofiber in this kind of FEC-additive electrolyte for SIBs. A high reversible capacity of 345–350 mAh·g<sup>-1</sup> at 0.2C, excellent capacity retention for more than 200 cycles (Fig. 6i) and enhanced reversible capacity of more than 110 mAh·g<sup>-1</sup> at the super high rate of 20C can be obtained.

### 3.2 Zn–Sb alloys

Orthorhombic ZnSb has a puckered layer structure, in which Zn and Sb atoms are connected by screw-typed layered chains. Inspired by the concept of quasi-intercalation of layered materials (orthorhombic ZnSb, orthorhombic P and rhombohedral As) (Fig. 7a), Park and Sohn [53] designed ZnSb anode materials with excellent electrochemical properties. Layered materials are readily transformed to amorphous composites by HEMM. Ex situ X-ray diffraction (XRD) results demonstrated during lithiation, Li is inserted into the puckered hexagonal channels which transform to regular hexagonal channels. And this phase transformation induces rearrangement to the layered Zn–Sb planes and periodic Li arrays through the cleavage and recombination of puckered Zn–Sb chains (Fig. 7b). The milled ZnSb/C nanocomposite electrode shows an excellent electrochemical stability with high gravimetric capacity of 520 mAh·g<sup>-1</sup> even after 200 cycles, and the capacity retention after 200 cycles corresponds to approximately 88% of the first discharge capacity (Fig. 7c). The capacity retention of the ZnSb/C nanocomposite shows far

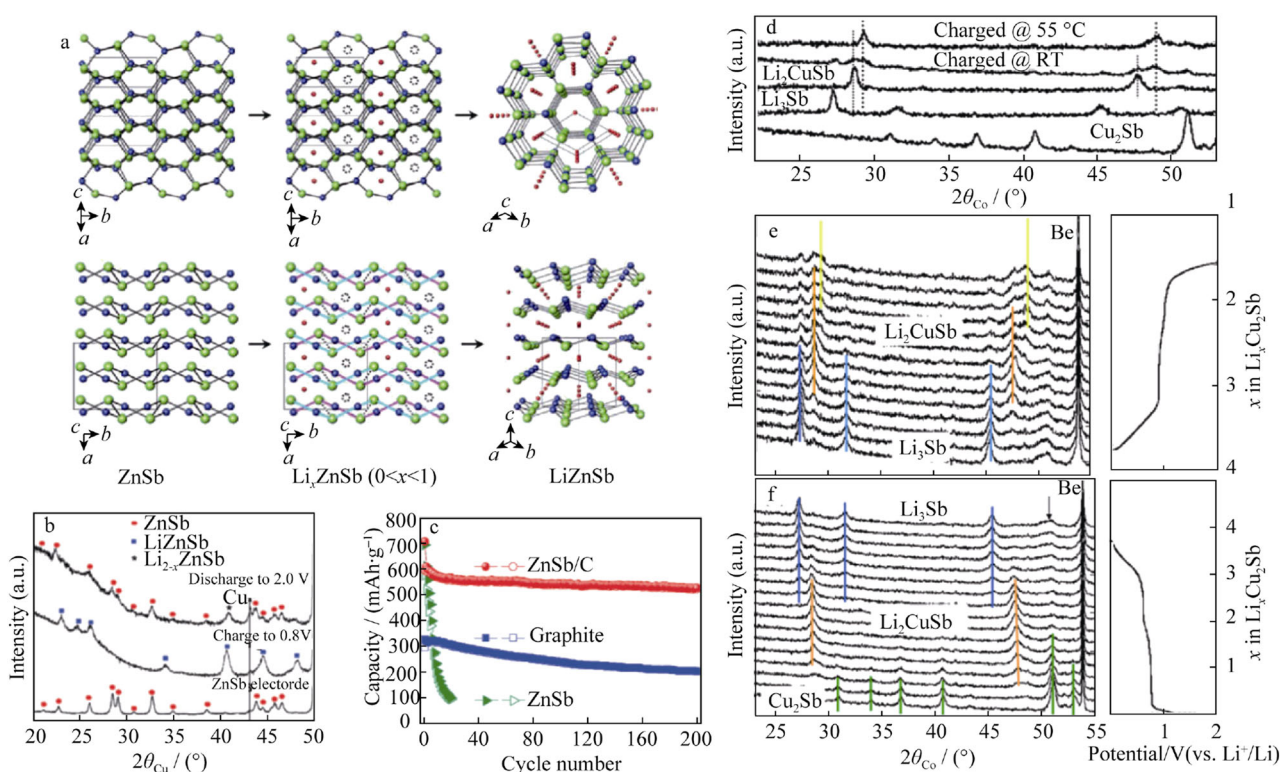


**Fig. 7** Mechanism of quasi-intercalation between ZnSb and LiZnSb **a**, ex situ XRD results of ZnSb electrode during the first charge (0.8 V) and discharge (2.0 V) **b**, comparison of cycle performances of ZnSb/C nanocomposite, ZnSb and graphite (MCMB) electrodes **c**, individual XRD patterns of Li<sub>3</sub>Sb, Li<sub>2</sub>CuSb and Cu<sub>2</sub>Sb charged at room temperature and Cu<sub>2</sub>Sb charged at 55 °C **d**, and in situ XRD patterns of Cu<sub>2</sub>Sb/carbon electrode collected during **e** charge and **f** discharge of a Cu<sub>2</sub>Sb/Li cell

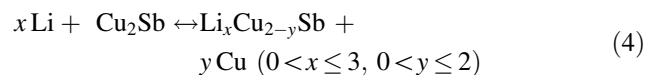
better electrochemical reversibility and cyclability than those of the ZnSb and MCMB electrodes.

Owing to their hollow structures, the ZnSb nanotubes depicted better Li-ion storage performance compared to ZnSb nanoparticles deposited under different conditions [68]. The ZnSb nanotubes depicted specific capacities of 406 and 350 mAh·g<sup>-1</sup> at 1C and 2C, respectively, which were 22 and 30% higher than those of ZnSb nanoparticles. A LIBs anode composed of interconnected ZnSb nanoflakes [95] depicted high discharge capacities and a stable performance with an initial discharge capacity of 735 mAh·g<sup>-1</sup> and an initial Coulombic efficiency of 85%. In addition, the ZnSb nanoflakes maintained a discharge capacity of 500 mAh·g<sup>-1</sup> with a Coulombic efficiency of 98% after 70 cycles at a current density of 100 mA·g<sup>-1</sup> (0.18C). The improved performance of the interconnected ZnSb nanoflakes is attributed to their open structure, with a large surface area and small crystal grains, to facilitate the diffusion of Li ions and to buffer the large volume swings during the lithium intercalation process.

Zn<sub>4</sub>Sb<sub>3</sub> also has gained much research interest as a promising anode in LIBs and SIBs. Zhao and Cao [52] firstly studied Zn<sub>4</sub>Sb<sub>3</sub> as a potential material for negative electrodes of lithium-ion batteries. It was found that the reversible capacity of ball-milled Zn<sub>4</sub>Sb<sub>3</sub> in the first cycle reached 507 mAh·g<sup>-1</sup> and increased up to 580 mAh·g<sup>-1</sup> when the alloy was ball-milled with about 11.8 wt% graphite additives. Zheng et al. demonstrated the CVD growth of several novel 1D Zn<sub>4</sub>Sb<sub>3</sub> structures, including nanotubes, nanowires and nanorods, directly on a Cu foil [76]. The 1D transport nature and the tubular structures of the obtained Zn<sub>4</sub>Sb<sub>3</sub> nanotubes offer excellent anode capacity and cycling stability, while the direct deposition of electroactive materials on Cu foils allows for direct battery assembly. As proof of concept, the anodes made of Zn<sub>4</sub>Sb<sub>3</sub> nanotubes showed a high initial discharge capacity of 1160 mAh·g<sup>-1</sup> at 100 mA·g<sup>-1</sup> and maintained a reversible capacity of 450 mAh·g<sup>-1</sup> after 100 cycles.

### 3.3 Cu–Sb-based alloys

In most of the literature, Li–Cu<sub>2</sub>Sb cells are reported to be operated by a mechanism involving lithium insertion/copper extrusion reactions as illustrated by the following reaction [70, 96]:



Specifically, in the first step, Li is inserted into Cu<sub>2</sub>Sb associated with Cu extrusion, which initiates a phase transition to a lithiated Li<sub>x</sub>Cu<sub>2-y</sub>Sb (0 < x ≤ 2 and 0 < y ≤ 1). And the intermediate product after the first step is Li<sub>2</sub>CuSb.

In the second step, further lithiation would result in the displacement of the remaining Cu to yield Li<sub>2+z</sub>Cu<sub>1-z</sub>Sb here 0 < z ≤ 1 with the final product Li<sub>3</sub>Sb. The lithium insertion/metal extrusion phenomena are similar to those observed in Li–Cu<sub>6</sub>Sn<sub>5</sub> system [97] and Li–InSb system [98].

However, Tarascon et al. claimed the structural reversibility of the Cu<sub>2</sub>Sb electrode can be obtained in two special cases [99]: (1) when the particle size of Cu<sub>2</sub>Sb is small and when the powders are ball-milled with carbon and (2) when Li<sub>2</sub>CuSb is used as the starting material and some Sb is lost from the electrode during charge (Fig. 7d–f). Through a different arsenal of characterization techniques, they emphasized the role of the particle size, electrode preparation and temperature on the reversibility of the electrochemical reaction. Tarascon et al. demonstrated that the grain growth of the extruded Cu atoms during discharge and retention of electronic conductivity must be carefully controlled to ensure good cycle life. Such as in a Cu<sub>2</sub>Sb–Al<sub>2</sub>O<sub>3</sub>–C composite [100], after 500 cycles, Cu<sub>2</sub>Sb–Al<sub>2</sub>O<sub>3</sub>–C has transformed into well-defined, 2–10 nm-sized crystalline particles that are almost entirely separated from one another and are surrounded by a matrix of Al<sub>2</sub>O<sub>3</sub> and C. After 50 cycles, Cu<sub>2</sub>Sb–C has almost completely transformed into crystalline spherical particles that are embedded in a carbon matrix.

In most of Sb-based intermetallic compounds, when one of the phases is deformed, the other phase may retain the stability and maintains good electric contact during the alloying–de-alloying processes. Therefore, some amorphous buffer or hollow structure can accommodate the volume expansion and enhance the electrochemical performance. For instance, the amorphous carbon layers in Sb–Cu<sub>2</sub>Sb@C composite [101] could remit the damage of electrode resulted from large volume expansion. The as-synthesized composites display an initial reversible capacity of 602 mAh·g<sup>-1</sup> and maintain 461 mAh·g<sup>-1</sup> after 60 cycles. Hollow Cu<sub>2</sub>Sb@C core–shell nanocomposite [32] showed good cycling performance, because the drastic volume change of Cu<sub>2</sub>Sb alloy particles was suppressed by the carbon layer and numerous pores during the charge and discharge reaction. At the 100th cycle, the discharge capacity of the hollow core–shell Cu<sub>2</sub>Sb@C nanoparticle electrode was 384.8 mAh·g<sup>-1</sup>.

### 3.4 Co–Sb alloys

Tirado and coworker investigated the electrochemical reaction of lithium with the skutterudite CoSb<sub>3</sub> in 1999 [102]. In their study, Li–CoSb<sub>3</sub> cell was established by using crystalline solid CoSb<sub>3</sub> with skutterudite structure as anode and a LiClO<sub>4</sub> + PC electrolyte. The first discharge involves the irreversible decomposition of the solid to

noncrystalline cobalt and  $\text{Li}_3\text{Sb}$  alloy. On cycling, the reversible extraction/insertion of lithium in the antimony alloy takes place. Part of the irreversible capacity is ascribable to the formation of a passivating film on the surface of the electrode material. It is found that the capacity retention is better than that of pure antimony electrodes, probably due to the dispersion of the metal caused by the decomposition of skutterudite solid  $\text{CoSb}_3$ . Afterward, Zhao et al. conducted an ex situ studies of  $\text{CoSb}_3$  compound as the anode material for LIBs [103]. Their results revealed that when  $\text{CoSb}_3$  is intercalated by Li ions, it decomposes into Co and Sb first, followed by the formation of the  $\text{Li}_3\text{Sb}$  phase, which is dispersed in the Co matrix. When Li ions are removed from  $\text{Li}_3\text{Sb}$ , Co and Sb atoms cannot reconstruct  $\text{CoSb}_3$ , while the Li/Sb alloying and de-alloying processes are reversible.

Nevertheless, Tarascon et al. [104] insisted that the reconstruction of  $\text{CoSb}_3$  during charge was possible on the basis of in situ XRD microscopy and magnetic measurements. More importantly, he declared that this phase reacts with more than 9.5 lithium in a two-step process, consisting of the uptake of nine Li at a constant voltage close to 0.6 V, and of about one lithium over the final voltage decay to 0.01 V (Fig. 8a). Upon recharge, only eight lithium can be extracted. Although these materials can reversibly

uptake about 8 lithium, they are of negligible value, since their capacity rapidly decays with cycling, independent of the electrode processing (Fig. 8b).

Some examples studied the lithium storage behavior of Co–Sb alloy anode. The reversible capacity of  $\text{CoSb}_3/\text{MWCNT}$  [29] as LIBs anode reaches  $312 \text{ mAh}\cdot\text{g}^{-1}$  at the first cycle and remains above  $265 \text{ mAh}\cdot\text{g}^{-1}$  after 30 cycles. A highly ordered  $\text{CoSb}$  nanowire array structures [66] have a charge–discharge capacity of around  $200 \text{ mAh}\cdot\text{g}^{-1}$ , with a Coulombic efficiency of 86% and a capability retention rate as low as 28% after 10 cycles. Park et al. [105] reported a  $\text{CoSb}_2/\text{C}$  nanocomposite electrode comprising of disproportionated nanocrystalline  $\text{CoSb}$ , amorphous Sb and an amorphous carbon matrix showed excellent electrochemical properties, such as a high energy density (first charge:  $578 \text{ mAh}\cdot\text{g}^{-1}$  or  $2895 \text{ mAh}\cdot\text{cm}^{-3}$ ), cycling durability over 100 cycles (above  $490 \text{ mAh}\cdot\text{g}^{-1}$  or  $2450 \text{ mAh}\cdot\text{cm}^{-3}$ ), high initial Coulombic efficiency (78.1%) and a fast rate capability (1C:  $472 \text{ mAh}\cdot\text{g}^{-1}$ , 3C:  $415 \text{ mAh}\cdot\text{g}^{-1}$ ). Yan et al. introduced an interesting controlled synthesis of Sb nanostructures and their conversion to  $\text{CoSb}_3$  nanoparticle chains for LIBs electrode [106]. The capacity of  $\text{CoSb}_3$  NPs chain was  $468 \text{ mAh}\cdot\text{g}^{-1}$  during the second cycle, which dropped to  $421 \text{ mAh}\cdot\text{g}^{-1}$  during the 70th cycle at a rate of 0.2C.

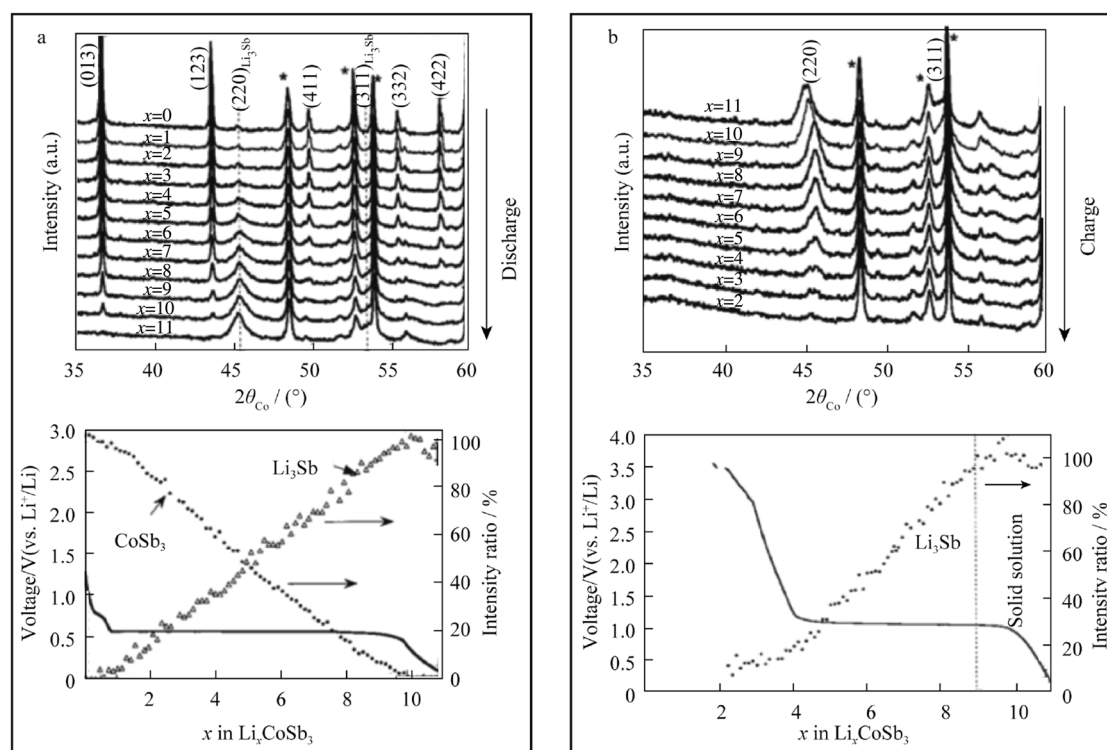


**Fig. 8** In situ X-ray powder patterns collected (upper) and amplitude evolution for relative intensity ratio of diffraction peak of  $\text{CoSb}_3$  and  $\text{Li}_3\text{Sb}$  peaks (below) during **a** discharge and **b** charge of a  $\text{CoSb}_3/\text{Li}$  electrochemical cell

### 3.5 Ni–Sb alloys

Monconduit et al. firstly studied the electrochemical reaction mechanism of lithium with NiSb<sub>2</sub> intermetallic material [107, 108]. It was shown that during the first discharge the orthorhombic NiSb<sub>2</sub> phase undergoes a pure conversion process ( $\text{NiSb}_2 + 6\text{Li}^+ + 6\text{e}^- \rightarrow \text{Ni} + 2\text{Li}_3\text{Sb}$ ). An advanced NiSb hollow spheres anode [74] gave the best electrochemical performances for NiSb alloy materials as LIBs anode so far with a high reversible capacity of 420 mAh·g<sup>-1</sup> after 50 cycles, close to its theoretical capacity (446 mAh·g<sup>-1</sup>). The thin shells greatly shorten the distances for Li<sup>+</sup> diffusion; the void space effectively accommodates the dramatic volume change and alleviates the strain during lithiation–delithiation.

A unique 3D interconnected NiSb hollow spheres [15] were prepared as SIBs anode. Compared to pure Sb electrode, the capacity retention of the obtained electrode was greatly improved. For SIBs, NiSb hollow spheres exhibit highly stable and substantial discharge capacities of 400, 372 and 230 mAh·g<sup>-1</sup> after 150 cycles at 1, 5 and 10C, respectively (Fig. 9a). Moreover, a full Na<sub>0.4</sub>Mn<sub>0.54</sub>Co<sub>0.46</sub>O<sub>2</sub>/NiSb battery shows a charge and discharge capacity of 451 and 301 mAh·g<sup>-1</sup>, respectively, at a current density of 300 mA·g<sup>-1</sup>. And it also displayed relatively good stability, retaining 75% of the initial discharge capacity after 20 cycles (Fig. 9b).

Apart from the aforesaid NiSb hollow sphere anode and 3D interconnected NiSb hollow sphere anode, other different Ni–Sb nanomaterials were also prepared as LIBs or SIBs anode, such as Ni<sub>5</sub>Sb<sub>2</sub> nanowire array [67], NiSb<sub>2</sub> powder [31] and NiSb particle [30]. Although these anodes deliver a high initial discharge capacity of 200–550 mAh·g<sup>-1</sup>, their cycle life is less than 30 cycles; therefore, further improvement on electrochemical stability should be addressed upon long-term cycling.

### 3.6 Other Sb-based alloys

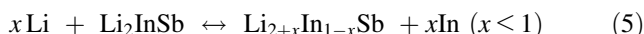
Besides the aforementioned typical Sb-based alloys, other Sb-based intermetallic compounds have also drawn much attention for LIBs or SIBs application, such as Mo<sub>3</sub>Sb<sub>7</sub> [109], Mn–Sb alloy [110–112], InSb [113–116], Ag–Sb alloy [117–120], Mg–Sb alloy [121, 122], TiSb<sub>2</sub> [123–125], VSb<sub>2</sub> [126], CrSb<sub>2</sub> [127, 128] and FeSb<sub>2</sub> [129–131]. Some original and insightful research has been achieved and illustrated as follows.

#### 3.6.1 Mo–Sb

Mo<sub>3</sub>Sb<sub>7</sub> thin films prepared by magnetron sputtering were evaluated as an anode material for LIBs and SIBs [109]. Excellent rate performance and good cycling are obtained in both cases. Indeed, with Li, a reversible capacity of 310 mAh·g<sup>-1</sup> is obtained at 100C (Fig. 10a) and a reversible capacity of 280 mAh·g<sup>-1</sup> is measured at 30C during the reaction with Na (Fig. 10b). The study of the changes in bulk structure by XRD shows that Li<sub>3</sub>Sb nanocrystallites can be formed at full discharge during the reaction with Li, whereas the electrode remains amorphous with Na. This is similar to the reaction of SnSb with Na but contrasts with the reaction of Cu<sub>2</sub>Sb, which can form Na<sub>3</sub>Sb nanodomains at full sodiation. The capacity retention can be improved by using FEC as Na-ion electrolyte additive.

#### 3.6.2 In–Sb

An intermetallic InSb compound with a zinc blende-type (diamond) structure as an anode for LIBs was reported. The reaction of InSb with Li was demonstrated as follows:



Although Vaughey et al. mentioned that the above results of InSb could open up possibilities for identifying other

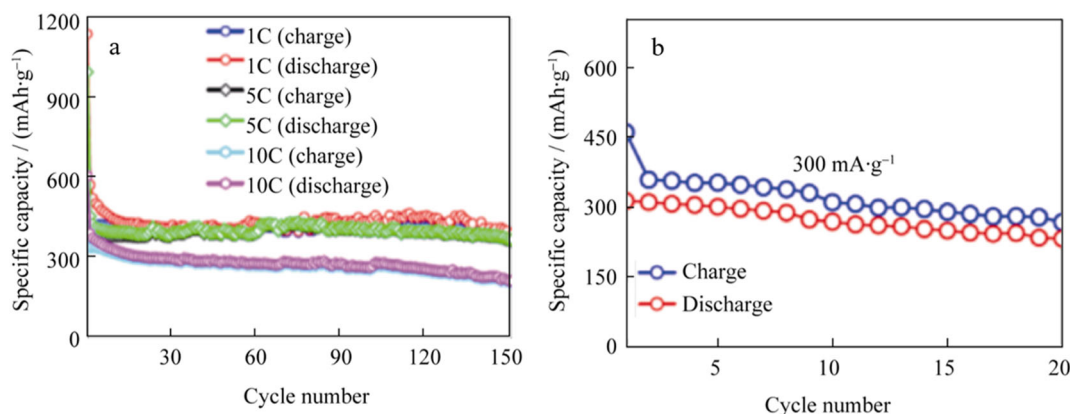


**Fig. 9** Capacity retention of 3D interconnected NiSb hollow nanospheres as anode for SIBs **a** and cycling performance of Na-ion full battery consisting of Na<sub>0.4</sub>Mn<sub>0.54</sub>Co<sub>0.46</sub>O<sub>2</sub> cathode and NiSb anode **b**

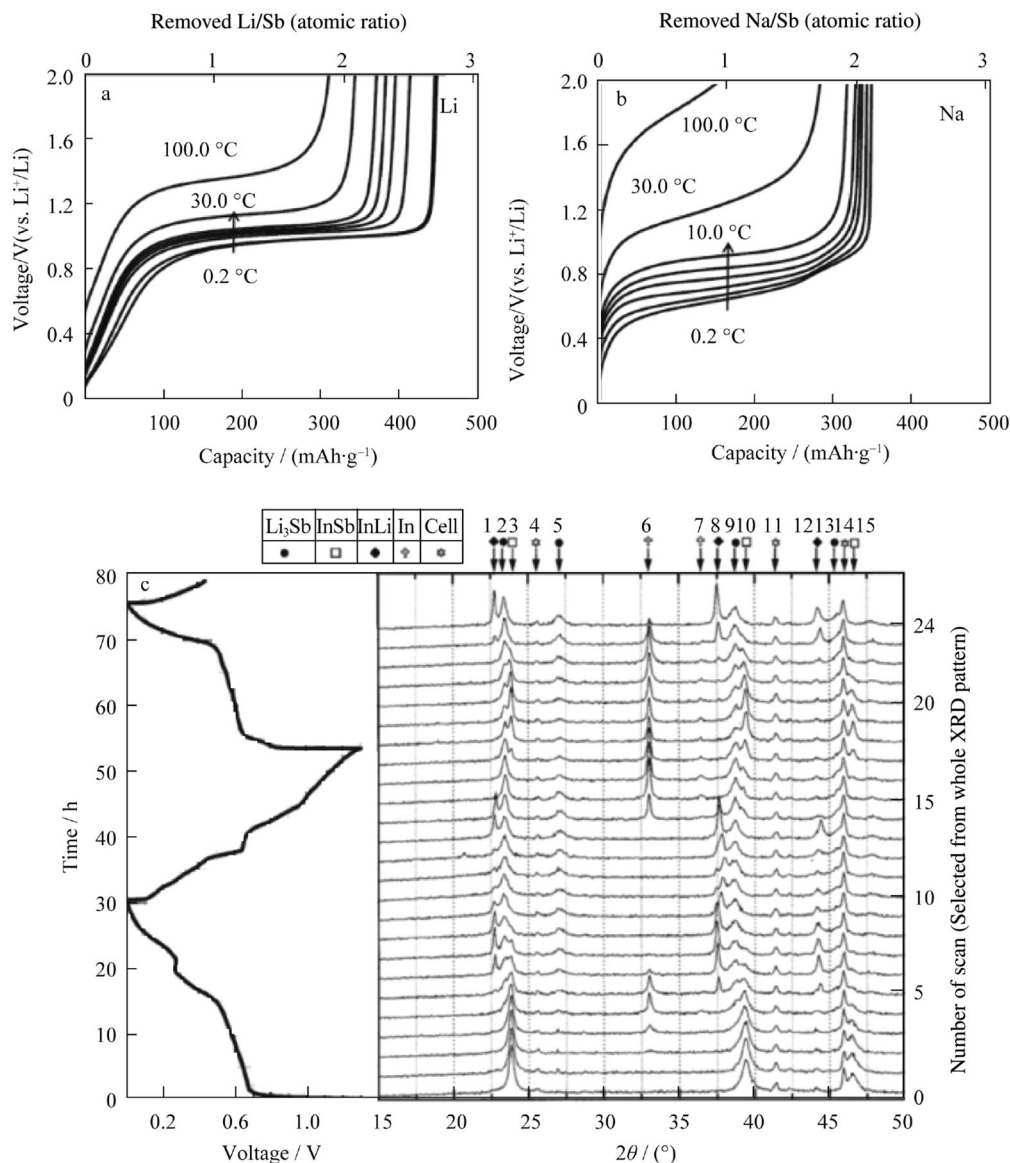


**Fig. 10** Rate performance of  $\text{Mo}_3\text{Sb}_7$  film electrodes during charge (ion removal) measured from 0.2C to 100.0C in **a** LIBs and **b** SIBs (Li/Sb and Na/Sb being mole ratio); **c** in situ XRD patterns of InSb electrode of a Li/InSb cell cycled between 0 and 1.3 V

zinc blende insertion electrodes [115], Hewitt et al. [113] suggested another reaction mechanism of InSb electrodes based on their in situ XRD results (Fig. 10c). It is found that only 0.27 Li atoms per InSb may be intercalated followed by decomposition of the ternary phase. Li intercalation was possible with only about 5% of the overall capacity, and it appears that the reactivity of the elements was the most significant factor in determining the performance of InSb intercalation host.

### 3.6.3 Mn–Sb

Jumas et al. studied Li insertion mechanisms in transition metal antimony compounds as negative electrodes for LIBs [111]. MSb (M = Ni, Co, Fe, Mn) alloys with a

NiAs-type structure were synthesized by ceramic route and evaluated as a negative electrode material for rechargeable lithium batteries. Electrochemical tests demonstrated that initial charge and discharge capacities of this material were 390 and 330  $\text{mAh}\cdot\text{g}^{-1}$ , respectively. Specifically, ex situ XRD patterns of MnSb electrodes showed that  $\text{LiMnSb}$  and  $\text{Li}_3\text{Sb}$  were successively formed during lithium insertion (Fig. 11a, b). The  $^{121}\text{Sb}$  Mössbauer spectra show that the insertion mechanism during discharge involves the formation of several lithium-containing compounds such as  $\text{LiMnSb}$ ,  $\text{Li}_3\text{Sb}$  with manganese extrusion (Fig. 11c, d). During the subsequent charge, a more complex mechanism occurs involving MnSb, modified  $\text{LiMnSb}$  alloy and metallic Sb formation.

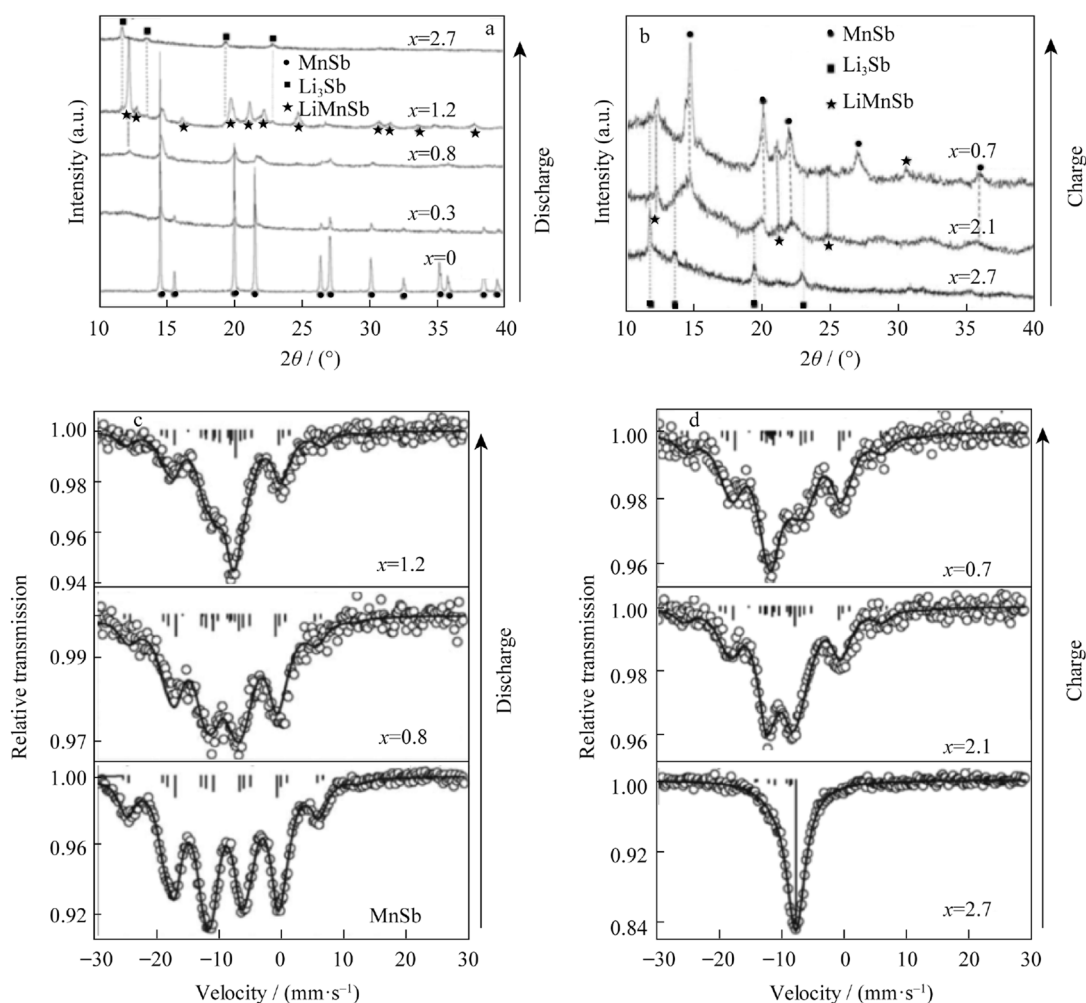


**Fig. 11** XRD patterns of MnSb **a** discharged at 0.2 V and **b** charged at 1.4 V;  $^{121}\text{Sb}$  Mössbauer spectra of MnSb **c** discharged and **d** charged

#### 4 Conclusion

In summary, this review highlights the recent progress in improving and understanding the electrochemical performance of various Sb-based intermetallic compounds anode. The developments of synthesis and construction of Sb-based intermetallic compounds are systematically summarized. The electrochemical performance of various Sb-based intermetallic compound anodes is compared in LIBs or SIBs. Notably, the rational construction of advanced anode with unique structures has been proven to be an effective approach to enhance the electrochemical performance of various Sb-based intermetallic compound anodes. Diverse nanostructures have been prepared for Sb-based alloy anode, including hollow spheres, nanowires/nanotubes/nanorods, porous particles and hybrid nanocomposites. As emphasized in this review, the success of nanostructure engineering on these Sb alloy materials depends on the comprehensive combination of various basic general strategies.

For Sb-based intermetallic alloy anode, although the electrochemical performances have been addressed and enhanced to some extent, great issues still remain as a challenge to be concerned: the irreversible capacity loss for the first cycle and fast capacity decay, serious aggregation of active particles during alloying/de-alloying process, the decomposition of electrolyte, the unclear reaction mechanism for some of Sb-based alloy anode and so forth.

The key issue with Sb-based intermetallic anode to become a commercial technology is the severe structural degradation caused by huge volume expansion. Therefore, the main ideas of developing high performance of Sb-based intermetallic compound anode involve the rational design of nanostructured advanced anode and the probe of its uncovered lithium/sodium storage mechanism. At this stage, developing facile, efficient and controllable synthesis of novel Sb-based nanostructures is still urgently demanded. Moreover, chemistry opens up a possibility to explore potential new-type Sb-based beyond metallic compounds, such as Sb-based chalcogenides [132, 133],

Sb-based oxides [134, 135] and multi-component Sb-based alloys [136, 137]. And challenges and breakthroughs might lie ahead bearing the deeper understanding of solid-state physics. With respect to its unclear reaction mechanism, some ex situ, operando measurements are highly considered to provide useful and detailed information upon the electrochemical reaction mechanisms. It can be confidently anticipated that this kind of high-capacity Sb-based intermetallic compound anode will be developed in the near future through continuous efforts for next-generation high-performance LIBs and SIBs.

**Acknowledgements** This work was financially supported by the National Key Research and Development Program of China (No. 2016YFA0202603), the National Basic Research Program of China (No. 2013CB934103), the Program of Introducing Talents of Discipline to Universities (No. B17034), the National Natural Science Foundation of China (No. 51521001), the National Natural Science Fund for Distinguished Young Scholars (No. 51425204), the Fundamental Research Funds for the Central Universities (Nos. 2016III001 and 2016-JL-004), and the China Scholarship Council (No. 201606955096).

## References

- Armand M, Tarascon JM. Building better batteries. *Nature*. 2008;451(7179):652.
- Goodenough JB, Park KS. The Li-ion rechargeable battery: a perspective. *J Am Chem Soc*. 2013;135(4):1167.
- Mai L, Tian X, Xu X, Chang L, Xu L. Nanowire electrodes for electrochemical energy storage devices. *Chem Rev*. 2014;114(23):11828.
- Slater MD, Kim D, Lee E, Johnson CS. Sodium-ion batteries. *Adv Funct Mater*. 2013;23(26):947.
- Kim SW, Seo DH, Ma X, Ceder G, Kang K. Electrode materials for rechargeable sodium-ion batteries: potential alternatives to current lithium-ion batteries. *Adv Energy Mater*. 2012;2(7):710.
- Palomares V, Serras P, Villaluenga I, Hueso KB, Carretero-gonzález J, Rojo T. Na-ion batteries, recent advances and present challenges to become low cost energy storage systems. *Energy Environ Sci*. 2012;5(3):5884.
- Wang X, Niu C, Meng J, Ping H, Xu X, Wei X, Zhou L, Zhao K, Luo W, Yan M, Mai L. Novel  $K_3V_2(PO_4)_3/C$  bundled nanowires as superior sodium-ion battery electrode with ultrahigh cycling stability. *Adv Energy Mater*. 2015;5(17):939.
- Han MH, Gonzalo E, Singh G, Rojo T. A comprehensive review of sodium layered oxide: powerful cathode for Na-ion battery. *Energy Environ Sci*. 2014;8(1):81.
- Scrosati B, Hassoun J, Sun YK. Lithium-ion batteries. A look into the future. *Energy Environ Sci*. 2011;4(9):3287.
- Thackeray MM, Wolverton C, Isaacs ED. Electrical energy storage for transportation—approaching the limits of, and going beyond, lithium-ion batteries. *Energy Environ Sci*. 2012;5(7):7854.
- Farbod B, Cui K, Kalisvaart WP, Kupsta M, Zahiri B, Kohandehghan A, Lotfabad EM, Li Z, Luber EJ, Mitlin D. Anodes for sodium ion batteries based on tin–germanium–antimony alloys. *ACS Nano*. 2014;8(5):4415.
- Luo W, Zhang P, Wang X, Li Q, Dong Y, Hua J, Zhou L, Mai L. Antimony nanoparticles anchored in three-dimensional carbon network as promising sodium-ion battery anode. *J Power Sources*. 2016;304:340.
- Chen C, Fu K, Lu Y, Zhu J, Xue L, Hu Y, Zhang X. Use of a tin antimony alloy-filled porous carbon nanofiber composite as an anode in sodium-ion batteries. *RSC Adv*. 2015;5(39):30793.
- Ji L, Zhou W, Chabot V, Yu A, Xiao X. Reduced graphene oxide/tin-antimony nanocomposites as anode materials for advanced sodium ion batteries. *ACS Appl Mater Interfaces*. 2015;7(44):24895.
- Liu J, Yang Z, Wang J, Gu L, Maier J, Yu Y. Three-dimensionally interconnected nickel–antimony intermetallic hollow nanospheres as anode material for high-rate sodium-ion batteries. *Nano Energy*. 2015;16:389.
- Tran CCH, Autret C, Damas C, Claude-Montigny B, Santos-Peña J. An electrochemical study of  $Fe_{1.18}Sb_{1.82}$  as negative electrode for sodium ion batteries. *Electrochim Acta*. 2015;182(9):11.
- Yang J. Sub-microcrystalline Sn and Sn–SnSb powders as lithium storage materials for lithium-ion batteries. *Electrochem Solid State Lett*. 1999;2(4):161.
- Yang J, Takeda Y, Imanishi N, Yamamoto O. Ultrafine Sn and  $SnSb_{0.14}$  powders for lithium storage matrices in lithium-ion batteries. *J Electrochem Soc*. 1999;146(146):4009.
- Li H, Shi L, Lu W, Huang X, Chen L. Studies on capacity loss and capacity fading of nanosized SnSb alloy anode for Li-ion batteries. *J Electrochem Soc*. 2001;148(8):A915.
- Wang Z, Zhou L, Lou XW. Metal oxide hollow nanostructures for lithium-ion batteries. *ChemInform*. 2012;24(24):1903.
- Wang Y, Cao G. Developments in nanostructured cathode materials for high-performance lithium-ion batteries. *Adv Mater*. 2008;20(12):2251.
- Ji L, Lin Z, Alcoutlabi M, Zhang X. Recent developments in nanostructured anode materials for rechargeable lithium-ion batteries. *Energy Environ Sci*. 2011;4(8):2682.
- Park CM, Kim JH, Kim H, Sohn HJ. Li-alloy based anode materials for Li secondary batteries. *ChemInform*. 2010;39(42):3115.
- Obrovac MN, Chevrier VL. Alloy negative electrodes for Li-ion batteries. *Chem Rev*. 2014;114(23):11444.
- Zhang WJ. A review of the electrochemical performance of alloy anodes for lithium-ion batteries. *J Power Sources*. 2011;196(1):13.
- Xie J, Cao GS, Zhao XB, Zhong YD, Zhao MJ. Electrochemical performances of nanosized intermetallic compound  $CoSb_2$  prepared by the solvothermal route. *J Electrochem Soc*. 2004;151(11):A1905.
- Xie J, Zhao XB, Cao GS, Zhong YD, Zhao MJ, Tu JP. Solvothermal synthesis of nanosized  $CoSb_2$  alloy anode for Li-ion batteries. *Electrochim Acta*. 2005;50(9):1903.
- Xie J, Zhao XB, Cao GS, Zhao MJ, Su SF. Solvothermal synthesis and electrochemical performances of nanosized  $CoSb_3$  as anode materials for Li-ion batteries. *J Power Sources*. 2005;140(2):350.
- Xie J, Zhao XB, Cao GS, Zhao MJ. Electrochemical performance of  $CoSb_3$ /MWNTs nanocomposite prepared by in situ solvothermal synthesis. *Electrochim Acta*. 2005;50(13):2725.
- Xie J, Zhao XB, Yu HM, Qi H, Cao GS, Tu JP. Low temperature solvothermal synthesis of nanosized NiSb as a Li-ion battery anode material. *J Alloy Compd*. 2007;441(1–2):231.
- Xie J, Zhao XB, Cao GS, Zhao MJ, Su SF. Electrochemical Li-uptake properties of nanosized NiSb<sub>2</sub> prepared by solvothermal route. *J Alloy Compd*. 2005;393(1):283.
- He Y, Huang L, Li X, Xiao Y, Xu GL, Li JT, Sun SG. Facile synthesis of hollow  $Cu_2Sb@C$  core–shell nanoparticles as a superior anode material for lithium ion batteries. *J Mater Chem*. 2011;21(46):18517.

- [33] Sarakonsri T, Johnson CS. Solution route synthesis of InSb,  $\text{Cu}_6\text{Sn}_5$  and  $\text{Cu}_2\text{Sb}$  electrodes for lithium batteries. *J Power Sources*. 2006;153(2):319.
- [34] Ren J, He X, Pu W, Jiang C, Wan C. Chemical reduction of nano-scale  $\text{Cu}_2\text{Sb}$  powders as anode materials for Li-ion batteries. *Electrochim Acta*. 2006;52(4):1538.
- [35] Wang F, Zhao M, Song X. The improved electrochemical performance of SnSb-based alloy anode materials for Li-ion batteries. *J Alloy Compd*. 2009;472(1):55.
- [36] Shi L, Li H, Wang Z, Huang X, Chen L. Nano-SnSb alloy deposited on MCMB as an anode material for lithium ion batteries. *J Mater Chem*. 2001;11(5):1502.
- [37] Li H, Wang Q, Shi L, Chen L, Huang X. Nanosized SnSb alloy pinning on hard non-graphitic carbon spherules as anode materials for a Li ion battery. *Chem Mater*. 2001;14(1):103.
- [38] Chen WX, Lee JY, Liu Z. The nanocomposites of carbon nanotube with Sb and  $\text{SnSb}_{0.5}$  as Li-ion battery anodes. *Carbon*. 2003;41(5):959.
- [39] Wachtler M, Wagner MR, Schroettner H. Influence of the reductive preparation conditions on the morphology and on the electrochemical performance of Sn/SnSb. *Solid State Ionics*. 2004;168(1):51.
- [40] Park MS, Needham SA, Wang GX, Kang YM, Park JS, Dou SX, Liu HK. Nanostructured SnSb/carbon nanotube composites synthesized by reductive precipitation for lithium-ion batteries. *Chem Mater*. 2007;19(10):2406.
- [41] Li J, Ru Q, Hu S, Sun D, Zhang B, Hou X. Spherical nano-SnSb/MCMB/carbon core-shell composite for high stability lithium ion battery anodes. *Electrochim Acta*. 2013;113(4):505.
- [42] Fan S, Sun T, Rui X, Yan Q, Hng HH. Cooperative enhancement of capacities in nanostructured SnSb/carbon nanotube network nanocomposite as anode for lithium ion batteries. *J Power Sources*. 2012;201(1):288.
- [43] Tang X, Yan F, Wei Y, Zhang M, Wang T, Zhang T. Encapsulating Sn,Sb nanoparticles in multichannel graphene-carbon fibers as flexible anodes to store lithium ions with high capacities. *ACS Appl Mater Interfaces*. 2015;7(39):21890.
- [44] Nithyadharseni P, Reddy MV, Nalini B, Ravindran TR, Pillai BC, Kalpana M, Chowdari BVR. Electrochemical studies of CNT/Si-SnSb nanoparticles for lithium ion batteries. *Mater Res Bull*. 2015;70:478.
- [45] Zhang P, Wang Y, Wang Y, Ren X, Liu K, Chen S. Electrochemical lithiation and delithiation performance of SnSb-Ag/carbon nanotube composites for lithium-ion batteries. *J Power Sources*. 2013;233(4):166.
- [46] Li H, Wang Q, Shi L, Chen L, Huang X. Nanosized SnSb alloy pinning on hard non-graphitic carbon spherules as anode materials for a Li ion battery. *ChemInform*. 2002;14(13):103.
- [47] Seng KH, Guo ZP, Chen ZX, Liu HK. SnSb/Graphene composite as anode materials for lithium ion batteries. *J Comput Theor Nanos*. 2010;4(1):18.
- [48] Song S, Huo P, Fan W, Shi W, Yan Y. The facile synthesis of SnSb/graphene composites and their enhanced electrochemical performance for lithium-ion batteries. *Sci Adv Mater*. 2013;5(12):1801.
- [49] Walter M, Doswald S, Kovalenko MV. Inexpensive colloidal SnSb nanoalloys as efficient anode materials for lithium- and sodium-ion batteries. *J Mater Chem A*. 2016;4(18):7053.
- [50] He M, Walter M, Kravchyk KV, Erni R, Widmer R, Kovalenko MV. Monodisperse SnSb nanocrystals for Li-ion and Na-ion battery anodes: synergy and dissonance between Sn and Sb. *Nanoscale*. 2014;7(2):455.
- [51] Zhang DL. Processing of advanced materials using high-energy mechanical milling. *Prog Mater Sci*. 2004;49(3-4):537.
- [52] Zhao XB, Cao GS. A study of  $\text{Zn}_4\text{Sb}_3$  as a negative electrode for secondary lithium cells. *Electrochim Acta*. 2001;46(6):891.
- [53] Park CM, Sohn HJ. Quasi-intercalation and facile amorphization in layered ZnSb for Li-ion batteries. *Adv Mater*. 2010;22(1):47.
- [54] Park CM, Jeon KJ. Porous structured SnSb/C nanocomposites for Li-ion battery anodes. *Chem Commun*. 2010;47(7):2122.
- [55] Park CM, Sohn HJ. A mechano- and electrochemically controlled SnSb/C nanocomposite for rechargeable Li-ion batteries. *Electrochim Acta*. 2009;54(26):6367.
- [56] Leibowitz J, Allcorn E, Manthiram A. SnSb-TiC-C nanocomposite alloy anodes for lithium-ion batteries. *J Power Sources*. 2015;279:549.
- [57] Darwiche A, Sougrati MT, Fraise B, Stievano L, Monconduit L. Facile synthesis and long cycle life of SnSb as negative electrode material for Na-ion batteries. *Electrochem Commun*. 2013;32(32):18.
- [58] Xiao L, Cao Y, Xiao J, Wang W, Kovarik L, Nie Z, Liu J. High capacity, reversible alloying reactions in SnSb/C nanocomposites for Na-ion battery applications. *Chem Commun*. 2012;48(27):3321.
- [59] Kim IT, Kim SO, Manthiram A. Effect of TiC addition on SnSb-C composite anodes for sodium-ion batteries. *J Power Sources*. 2014;269(3):848.
- [60] Tian Q, Zhang Z, Yang L, Hirano SI. Fabrication of mesoporous titanium dioxide/tin dioxide/carbon hollow microspheres as high performance anode for lithium-ion batteries. *J Power Sources*. 2015;279:528.
- [61] Wang M, Zhao H, He J, Wang R, Chen J, Chen N. Preparation and electrochemical performance of CoSb alloy anode material for Li-ion batteries. *J Alloy Compd*. 2009;484(1-2):864.
- [62] Park CM, Sohn HJ. Electrochemical characteristics of TiSb<sub>2</sub> and Sb/TiC/C nanocomposites as anodes for rechargeable Li-Ion batteries. *J Electrochem Soc*. 2010;157(1):A46.
- [63] Simonin L, Lafont U, Kelder EM. SnSb micron-sized particles for Li-ion batteries. *J Power Sources*. 2008;180(2):859.
- [64] Guo H, Zhao H, Jia X, Qiu W, Cui F. Synthesis and electrochemical characteristics of Sn-Sb-Ni alloy composite anode for Li-ion rechargeable batteries. *Mater Res Bull*. 2007;42(5):836.
- [65] Yang T, Wang H, Xu J, Wang L, Song WC, Mao Y, Ma J. Preparation of a Sb/Cu<sub>2</sub>Sb/C composite as an anode material for lithium-ion batteries. *RSC Adv*. 2016;6(82):78959.
- [66] Yang YW, Liu F, Li TY, Chen YB, Wu YC, Kong MG. Electrochemical performance of template-synthesized CoSb nanowires array as an anode material for lithium ion batteries. *Scripta Mater*. 2012;66(7):495.
- [67] Yang YW, Li TY, Liu F, Zhu WB, Li XL, Wu YC, Kong MG. Electrodeposition of Ni<sub>5</sub>Sb<sub>2</sub> nanowires array and its application as a high-performance anode material for lithium ion batteries. *Microelectron Eng*. 2013;104:1.
- [68] Saadat S, Zhu J, Shahjamali MM, Maleksaeedi S, Tay YY, Tay BY, Hng HH, Ma J, Yan Q. Template free electrochemical deposition of ZnSb nanotubes for Li ion battery anodes. *Chem Commun*. 2011;47(35):9849.
- [69] Bryngelsson H, Eskhult J, Nyholm L, Edström K. Thin films of Cu<sub>2</sub>Sb and Cu<sub>9</sub>Sb<sub>2</sub> as anode materials in Li-ion batteries. *Electrochim Acta*. 2008;53(24):7226.
- [70] Mosby JM, Prieto AL. Direct electrodeposition of Cu<sub>2</sub>Sb for lithium-ion battery anodes. *J Am Chem Soc*. 2008;130(32):10656.
- [71] Sun Y, Xia Y. Alloying and dealloying processes involved in the preparation of metal nanoshells through a galvanic replacement reaction. *Nano Lett*. 2003;3(11):1569.
- [72] Au L, Lu X, Xia Y. A comparative study of galvanic replacement reactions involving ag nanocubes and  $\text{AuCl}_2^-$  or  $\text{AuCl}_4^-$ . *Adv Mater*. 2008;20(13):2517.

- [73] Oh MH, Hyeon T. Galvanic replacement reactions in metal oxide nanocrystals. *Science*. 2013;340(6135):964.
- [74] Hou H, Cao X, Yang Y, Fang L, Pan C, Yang X, Song W, Ji X. NiSb alloy hollow nanospheres as anode materials for rechargeable lithium ion batteries. *Chem Commun*. 2014;50(60):8201.
- [75] Chen J, Yin Z, Sim D, Tay YY, Zhang H, Ma J, Hng HH, Yan Q. Controlled CVD growth of Cu–Sb alloy nanostructures. *Nanotechnology*. 2011;22(32):325602.
- [76] Xu J, Wu H, Wang F, Xia Y, Zheng G. Zn<sub>4</sub>Sb<sub>3</sub> nanotubes as lithium ion battery anodes with high capacity and cycling stability. *Adv Energy Mater*. 2013;3(3):286.
- [77] Li L, Seng KH, Li D, Xia Y, Liu HK, Guo Z. SnSb@carbon nanocable anchored on graphene sheets for sodium ion batteries. *Nano Res*. 2014;7(10):1466.
- [78] Niu C, Meng J, Wang X, Han C, Yan M, Zhao K, Xu X, Ren W, Zhao Y, Xu L, Zhang Q, Zhao D, Mai L. General synthesis of complex nanotubes by gradient electrospinning and controlled pyrolysis. *Nat Commun*. 2015;6:7402.
- [79] Ren W, Zheng Z, Luo Y, Chen W, Niu C, Zhao K, Yan M, Zhang L, Meng J, Mai L. An electrospun hierarchical LiV<sub>3</sub>O<sub>8</sub> nanowire-in-network for high-rate and long-life lithium batteries. *J Mater Chem A*. 2015;3(39):19850.
- [80] Shiva K, Rajendra HB, Bhattacharyya AJ. Electrospun SnSb crystalline nanoparticles inside porous carbon fibers as a high stability and rate capability anode for rechargeable batteries. *Chem Plus Chem*. 2014;80(3):516.
- [81] Ji L, Gu M, Shao Y, Li X, Engelhard MH, Arey BW, Wang W, Nie Z, Xiao J, Wang C, Zhang J, Liu J. Controlling SEI formation on SnSb-porous carbon nanofibers for improved Na ion storage. *Adv Mater*. 2014;26(18):2901.
- [82] Niu X, Zhou H, Li Z, Shan X, Xia X. Carbon-coated SnSb nanoparticles dispersed in reticular structured nanofibers for lithium-ion battery anodes. *J Alloy Compd*. 2015;620:308.
- [83] Caillat T, Fleurial JP, Borshchevsky A. Preparation and thermoelectric properties of semiconducting Zn<sub>4</sub>Sb<sub>3</sub>. *J Phys Chem Solids*. 1997;58(7):1119.
- [84] Zhao X, Cao G, Li T. Electrochemical properties of Zn<sub>4</sub>Sb<sub>3</sub> as anode materials for lithium-ion batteries. *J Mater Sci Lett*. 2000;19(10):851.
- [85] Zhao X, Cao G, Lv C, Zhang L, Hu S, Zhu T, Zhou B. Electrochemical properties of some Sb or Te based alloys for candidate anode materials of lithium-ion batteries. *J Alloy Compd*. 2001;315(1):265.
- [86] Baggetto L, Marszewski M, Górka J, Jaroniec M, Veith GM. AlSb thin films as negative electrodes for Li-ion and Na-ion batteries. *J Power Sources*. 2013;243(1):699.
- [87] Baggetto L, Allcorn E, Unocic RR, Manthiram A, Veith GM. Mo<sub>3</sub>Sb<sub>7</sub> as a very fast anode material for lithium-ion and sodium-ion batteries. *J Mater Chem A*. 2013;1(37):11163.
- [88] Yang J, Takeda Y, Imanishi N, Ichikawa T, Yamamoto O. SnSb<sub>x</sub> based composite electrodes for lithium ion cells. *Solid State Ionics*. 2000;135(1):175.
- [89] Yang J, Takeda Y, Imanishi N, Xie JY, Yamamoto O. Intermetallic SnSb<sub>x</sub> compounds for lithium insertion hosts. *Solid State Ionics*. 2000;133(3–4):189.
- [90] Yoshida K, Sano Y, Tomii Y. Study on microstructural deformation of working Sn and SnSb anode particles for Li-ion batteries by in situ transmission X-ray microscopy. *J Phys Chem C*. 2011;115(44):22040.
- [91] Baggetto L, Hah HY, Jumas JC, Johnson CE, Johnson JA, Keum JK, Bridges CA, Veith GM. The reaction mechanism of SnSb and Sb thin film anodes for Na-ion batteries studied by X-ray diffraction, <sup>119</sup>Sn and <sup>121</sup>Sb Mössbauer spectroscopies. *J Power Sources*. 2014;267(267):329.
- [92] Xie J, Song W, Zheng Y, Liu S, Zhu T, Cao G, Zhao X. Preparation and Li-storage properties of SnSb/graphene hybrid nanostructure by a facile one-step solvothermal route. *Int J Smart Nano Mater*. 2011;2(4):1.
- [93] Birrozzi A, Maroni F, Raccichini R, Tossici R, Marassi R, Nobili F. Enhanced stability of SnSb/graphene anode through alternative binder and electrolyte additive for lithium ion batteries application. *J Power Sources*. 2015;294:248.
- [94] Tang X, Wei Y, Zhang H, Yan F, Zhuo M, Chen C, Xiao P, Liang J, Zhang M. The positive influence of graphene on the mechanical and electrochemical properties of Sn<sub>x</sub>Sb-graphene-carbon porous mats as binder-free electrodes for Li<sup>+</sup> storage. *Electrochim Acta*. 2015;186:223.
- [95] Saadat S, Tay YY, Zhu J, Teh PF, Maleksaedi S, Shahjamali MM, Shakerzadeh M, Srinivasan M, Tay BY, Hng HH, Ma J, Yan Q. Template-free electrochemical deposition of interconnected ZnSb nanoflakes for li-ion battery anodes. *Chem Mater*. 2011;23(4):1032.
- [96] Fransson LML, Vaughey JT, Benedek R, Edström K, Thomas JO, Thackeray MM. Phase transitions in lithiated Cu<sub>2</sub>Sb anodes for lithium batteries: an in situ X-ray diffraction study. *Electrochem Commun*. 2001;3(7):317.
- [97] Larcher D. In situ X-ray study of the electrochemical reaction of Li with Cu<sub>6</sub>Sn<sub>5</sub>. *J Electrochem Soc*. 2000;147(5):1658.
- [98] Johnson CS, Vaughey JT, Thackeray MM, Sarakonsri T, Hackney SA, Fransson L, Edström K, Thomas JO. Electrochemistry and in situ X-ray diffraction of InSb in lithium batteries. *Electrochem Commun*. 2000;2(8):595.
- [99] Morcrette M, Larcher D, Tarascon JM, Edström K, Vaughey JT, Thackeray MM. Influence of electrode microstructure on the reactivity of Cu<sub>2</sub>Sb with lithium. *Electrochim Acta*. 2007;52(17):5339.
- [100] Applestone DS. Cu<sub>2</sub>Sb–Al<sub>2</sub>O<sub>3</sub>–C nanocomposite alloy anodes for lithium-ion batteries. *ACS Appl Mater Interfaces*. 2014;6(14):10886.
- [101] He Y, Huang L, Li JT, Sun SG. Facile Synthesis of Sb–Cu<sub>2</sub>Sb@C core-shell nanocomposite as a superior anode material for lithium ion batteries. *J Interfaces Cytok Res*. 2013;34(3):148.
- [102] Alcántara R, Fernández-Madrigal FJ, Lavela P, Tirado JL, Jumas JC, Olivier-Fourcade J. Electrochemical reaction of lithium with the CoSb<sub>3</sub> skutterudite. *J Mater Chem*. 1999;9(10):2517.
- [103] Xie J, Zhao X, Cao G, Zhong Y, Zhao M. Ex-situ XRD studies of CoSb<sub>3</sub> compound as the anode material for lithium ion batteries. *J Electroanal Chem*. 2003;542(2):1.
- [104] Tarascon JM, Morcrette M, Dupont L, Chabre Y, Payen C, Larcher D, Pralong V. On the electrochemical reactivity mechanism of CoSb<sub>3</sub> vs. lithium. *J Electrochem Soc*. 2003;150(6):A732.
- [105] Park MG, Song JH, Sohn JS, Lee CK, Park CM. Co–Sb intermetallic compounds and their disproportionated nanocomposites as high-performance anodes for rechargeable Li-ion batteries. *J Mater Chem A*. 2014;2(29):11391.
- [106] Zhu J, Sun T, Chen J, Shi W, Zhang X, Lou X, Mhaisalkar S, Hng HH, Boey F, Ma J, Yan Q. Controlled synthesis of Sb nanostructures and their conversion to CoSb<sub>3</sub> nanoparticle chains for li-ion battery electrodes. *Chem Mater*. 2010;22(18):5333.
- [107] Villevieille C, Ionica-Bousquet CM, Ducourant B, Jumas JC, Monconduit L. NiSb<sub>2</sub> as negative electrode for Li-ion batteries: an original conversion reaction. *J Power Sources*. 2007;172(1):388.
- [108] Villevieille C, Ionica-Bousquet CM, Jumas JC, Monconduit L. <sup>121</sup>Sb Mössbauer study of the electrochemical reaction of NiSb<sub>2</sub> vs lithium. *Hyperfine Interact*. 2008;187(1):71.

- [109] Baggetto L, Allcorn E, Unocic R, Manthiram A, Veith G.  $\text{Mo}_3\text{Sb}_7$  as a very fast anode material for lithium-ion and sodium-ion batteries. *J Mater Chem A*. 2013;1(37):11163.
- [110] Fransson L, Vaughey J, Edström K, Thackeray M. Structural transformations in intermetallic electrodes for lithium batteries an in situ X-ray diffraction study of lithiated  $\text{MnSb}$  and  $\text{Mn}_2\text{Sb}$ . *J Electrochem Soc*. 2003;150(1):A86.
- [111] Ionica CM, Lippens PE, Fourcade JO, Jumas JC. Study of Li insertion mechanisms in transition metal antimony compounds as negative electrodes for Li-ion battery. *J Power Sources*. 2005;146(1):478.
- [112] Ionica-Bousquet CM, Womes M, Lippens PE, Olivier-Fourcade J, Ducourant B, Chadwick AV. Evaluation of structural and electrochemical properties of the  $\text{MnSb-Li}$  system as anode for Li-ion batteries. Heidelberg: ICAME 2005; 2006. 773.
- [113] Hewitt K, Beaulieu L, Dahn J. Electrochemistry of  $\text{InSb}$  as a Li insertion host: problems and prospects. *J Electrochem Soc*. 2001;148(5):A402.
- [114] Johnson C, Vaughey J, Thackeray M, Sarakonsri T, Hackney S, Fransson L, Edström K, Thomas JO. Electrochemistry and in situ X-ray diffraction of  $\text{InSb}$  in lithium batteries. *Electrochem Commun*. 2000;2(8):595.
- [115] Kropf A, Tostmann H, Johnson C, Vaughey J, Thackeray M. An in situ X-ray absorption spectroscopy study of  $\text{InSb}$  electrodes in lithium batteries. *Electrochem Commun*. 2001;3(5):244.
- [116] Tostmann H, Kropf A, Johnson C, Vaughey J, Thackeray M. In situ X-ray absorption studies of electrochemically induced phase changes in lithium-doped  $\text{InSb}$ . *Phys Rev B*. 2002;66(1):014106.
- [117] Vaughey J, Fransson L, Swinger H, Edström K, Thackeray M. Alternative anode materials for lithium-ion batteries: a study of  $\text{Ag}_3\text{Sb}$ . *J Power Sources*. 2003;119:64.
- [118] Zhao M, Zheng Q, Wang F, Qin Y, Song X. Nano-sized  $\text{SnSbAg}_x$  alloy anodes prepared by reductive co-precipitation method used as lithium-ion battery materials. *J Nanos Nanotechnol*. 2010;10(11):7025.
- [119] Yin J, Wada M, Tanase S, Sakai T. Electrode properties and lithiation/delithiation reactions of  $\text{Ag-Sb-Sn}$  nanocomposite anodes in Li-ion batteries. *J Electrochem Soc*. 2004;151(6):A867.
- [120] Rönnebro E, Yin J, Kitano A, Wada M, Tanase S, Sakai T. Reaction mechanism of a  $\text{Ag}_{36.4}\text{Sb}_{15.6}\text{Sn}_{48}$  nanocomposite electrode for advanced Li-ion batteries. *J Electrochem Soc*. 2005;152(1):A152.
- [121] Gnanapoongothai T, Murugan R, Palanivel B. First-principle study on lithium intercalated antimonides  $\text{Ag}_3\text{Sb}$  and  $\text{Mg}_3\text{Sb}_2$ . *Ionics*. 2015;21(5):1351.
- [122] Honda H, Sakaguchi H, Tanaka I, Esaka T. Anode behaviors of magnesium-antimony intermetallic compound for lithium secondary battery. *J Power Sources*. 2003;123(2):216.
- [123] Gómez-Cámer JL, Novák P. Polyacrylate bound  $\text{TiSb}_2$  electrodes for Li-ion batteries. *J Power Sources*. 2015;273:174.
- [124] Marino C, Sougrati MT, Gerke B, Pottgen R, Huo H, Ménétrier M, Grey CP, Monconduit L. Role of structure and interfaces in the performance of  $\text{TiSnSb}$  as an electrode for Li-ion batteries. *Chem Mater*. 2012;24(24):4735.
- [125] Sougrati MT, Fullenwarth J, Debenedetti A, Fraise B, Jumas JC, Monconduit L.  $\text{TiSnSb}$  a new efficient negative electrode for Li-ion batteries: mechanism investigations by operando-XRD and Mössbauer techniques. *J Mater Chem*. 2011;21(27):10069.
- [126] Larcher D, Beaulieu L, Mao O, George A, Dahn J. Study of the reaction of lithium with isostructural  $\text{A}_2\text{B}$  and various  $\text{Al}_x\text{B}$  alloys. *J Electrochem Soc*. 2000;147(5):1703.
- [127] Fernández-Madrigal FJ, Lavela P, Pérez-Vicente C, Tirado JL. Electrochemical reactions of polycrystalline  $\text{CrSb}_2$  in lithium batteries. *J Electroanal Chem*. 2001;501(1):205.
- [128] Park CM, Sohn HJ. Antimonides ( $\text{FeSb}_2$ ,  $\text{CrSb}_2$ ) with orthorhombic structure and their nanocomposites for rechargeable Li-ion batteries. *Electrochim Acta*. 2010;55(17):4987.
- [129] Villeveille C, Fraise B, Womes M, Jumas JC, Monconduit L. A new ternary  $\text{Li}_4\text{FeSb}_2$  structure formed upon discharge of the  $\text{FeSb}_2/\text{Li}$  cell. *J Power Sources*. 2009;189(1):324.
- [130] Baggetto L, Hah H-Y, Johnson CE, Bridges CA, Johnson JA, Veith GM. The reaction mechanism of  $\text{FeSb}_2$  as anode for sodium-ion batteries. *Phys Chem Chem Phys*. 2014;16(20):9538.
- [131] Villeveille C, Ionica-Bousquet C, Fraise B, Zitoun D, Womes M, Jumas JC, Monconduit L. Comparative study of  $\text{NiSb}_2$  and  $\text{FeSb}_2$  as negative electrodes for Li-ion batteries. *Solid State Ionics*. 2011;192(1):351.
- [132] Zhao Y, Manthiram A. Amorphous  $\text{Sb}_2\text{S}_3$  embedded in graphite: a high-rate, long-life anode material for sodium-ion batteries. *Chem Commun*. 2015;51(67):13205.
- [133] Luo W, Calas A, Tang C, Li F, Zhou L, Mai L. Ultralong  $\text{Sb}_2\text{Se}_3$  nanowire based free-standing membrane anode for lithium/sodium ion batteries. *ACS Appl Mater Interfaces*. 2016;8(51):35219.
- [134] Zhou X, Liu X, Xu Y, Dai Z, Bao J. An  $\text{SbO}_x/\text{reduced graphene oxide}$  composite as a high-rate anode material for sodium-ion batteries. *J Phys Chem C*. 2014;118(41):23527.
- [135] Sun Q, Ren Q, Li H, Fu Z. High capacity  $\text{Sb}_2\text{O}_4$  thin film electrodes for rechargeable sodium battery. *Electrochem Commun*. 2011;13(12):1462.
- [136] Chen X, Ru Q, Wang Z, Hou X, Hu S. Ternary  $\text{Sn-Sb-Co}$  alloy particles embedded in reduced graphene oxide as lithium ion battery anodes. *Mater Lett*. 2017;191:218.
- [137] Pang XJ, Tan CH, Dai XH, Wang X, Qi GW, Zhang SY. Performance enhancement of  $\text{Sn-Sb-Co}$  alloy film anode for lithium-ion batteries via post electrodisolution treatment. *J Appl Electrochem*. 2015;45(2):115.



**Li-Qiang Mai** is a Cheung Kong Chair Professor at Wuhan University of Technology (WUT). His current research interests focus on new nanomaterials for electrochemical energy storage and micro/nanoenergy devices. He has published 201 peer-review papers with more than 5300 citations. He received his Ph.D. from WUT in 2004. He carried out his postdoctoral research in the laboratory of Prof. Zhonglin Wang at Georgia Institute of

Technology in 2006–2007. He worked as advanced research scholar in the laboratory of Prof. Charles M. Lieber at Harvard University (2008–2011) and Prof. Peidong Yang's group at University of California, Berkeley (2017), respectively. He is the winner of the National Natural Science Fund for Distinguished Young Scholars. He won China Youth Science and Technology Award, National Ten Thousand Talent Plan of China and Guanghua Engineering Award. He is the guest editor of *Advanced Materials*, a member of advisory board of *Nano Research*, *Advanced Electronic Materials* and *Science China Materials*.